Large-Eddy Simulation of Transition Under Turbulence

Zhiyin Yang and Peter R. Voke
Department of Mechanical Engineering, University of Surrey,
Guildford GU2 5XH, United Kingdom

July 8, 1993

Abstract

A series of large-eddy simulations has been performed of a flat-plate boundary layer undergoing transition to turbulence under free-stream turbulence at levels of 3% and 6%. The properties of the simulated transition match those found experimentally: not only is the position and rate of transition in agreement with available data, but the mechanism of transition also appears to correspond closely, since disturbances seen in the laminar layer prior to transition are found in our simulations. We have also carried out some numerical experiments that indicate the key influence of the wall-normal component of free-stream turbulence intensity in provoking transition under turbulence.

Using the most reliable of our simulations, data has been gathered that allows the computation of all terms in the derived equations for the Reynolds stresses. Aspects of these balances are presented that allow new insights into the physical mechanisms at work, and the possible reason for poor predictions by many closure models. The importance of the wall-normal component of free-stream turbulence is confirmed. Wall damping functions for popular closure models used to predict transition have also been extracted from the large-eddy simulation, and are compared with popular two-equation closure approximations, showing that the most successful model for predicting this flow has some advantage over more recent models.

Contents

1 Introduction

The receptivity of the laminar boundary-layer to turbulence in the free stream is of major importance in turbomachinery flows, but is still only partly understood. It is known that this type of boundary-layer transition is affected by properties of the free-stream turbulence such as its anisotropy and length scale as well as its intensity. When the free-stream turbulence level is zero or very low, the transition occurs as two-dimensional Tollmien-Schlichting (T.S.) waves develop three-dimensional, nonlinear secondary instabilities which break down into turbulence. At levels of free-stream turbulence above about 0.5 to 1%, transition to turbulence becomes extremely rapid, and bypass transition takes place. The laminar boundary layer thus has an inbuilt receptivity to destabilization by external free-stream turbulence.

The natural transition of a flat plate boundary layer with zero pressure gradient has been simulated numerically by a number of workers, using either spectral methods (see the review by Kleiser and Zang, 1991) or finite differences (Fasel, Rist and Konselmann, 1990). Spatial simulations of two-dimensional disturbance development in Blasius flow were performed by Fasel (1976) and Murdock (1977). Three-dimensional spatial simulations of boundary transition have only become possible fairly recently owing to the computer speed and memory requirements, and usually periodic boundary conditions and Fourier expansions are used in the spanwise direction. K-type transition for the conditions of the experiment of Klebanoff *et al.* (1962) was simulated by Murdock (1986), who employed the modified vorticity/velocity-potential equations and used Chebyshev polynomial expansions in the streamwise and normal directions. He was unable to follow transition beyond about the one-spike stage since he used a high resolution on a domain extending over eight T.S. wavelength in the streamwise direction. More recently, Fasel, Rist and Konzelmann (1990) have simulated the early three-dimensional stages of both fundamental and subharmonic transition by employing the Navier-Stokes equations in vorticity-velocity formulation. Rist and Fasel (1991) have performed a numerical simulation of the vibrating-ribbon experiment by Kachanov *et al.* (1985) using the same method, and obtained good agreement between the simulation and the experiment. More recently Spalart (1993) has looked at transition induced by suction devices. Rai and Moin (1991) simulated boundary layer transition under turbulence in compressible flow using fifth-order-accurate upwind-biased differences for the convective terms and sixth-order-accurate central differences for the viscous terms. Their results indicated that the essential features of the transition process are captured.

Most transition simulations are performed using a temporal approach. Simulations of the fundamental type of transition in Blasius flow have been done by Orszag and Patera (1983) and by Wray and Hussaini (1984). Zang and Hussaini (1987, 1990), and Laurien and Kleiser (1989) have also studied the subharmonic type of transition. Spalart and Yang (1987) simulated a mixed type of transition developing from a

finite-amplitude two-dimensional wave and low-amplitude three-dimensional random disturbances. Generally numerical results are in good agreement with experimental data.

It is usually assumed that for such a computation a high level of numerical accuracy is required in order to reproduce the development of T.S. waves and their breakup through secondary and tertiary instabilities. Bypass transition appears to be different. Earlier work by the authors (Yang and Voke 1991, 1992) has shown that since the transition takes place early and rapidly, the detailed computation of the form of the instabilities is not crucial. Relatively coarse meshes and low-order but strictly conservative finite-volume methods correctly predict the position and speed of transition, and the presence and magnitude of disturbances in the laminar boundary layer prior to the eruption of true turbulence.

2 Methods

2.1 Finite-volume LES

The simulations have been prompted by the finding that behaviour very similar to bypass transition can be reproduced by conservative finite-volume simulations even on coarse meshes (Yang and Voke 1991), provided that the level of free-stream turbulence is high, suggesting that the conservation properties of the simulation algorithm are more important than the formal accuracy of the interpolations.

In the present work we continue to use the linear finite-volume approach. The method conserves momentum and mass to high accuracy volume by volume and globally, and conserves each component (u^2, v^2 and w^2) of kinetic energy and hence also the total flow kinetic energy to the same accuracy in the advection term, thus ensuring that the removal of energy from the simulation takes place entirely via the discrete approximation to the viscous term. These methods, which originated with Lilly (1965) and Bryant (1966), were used by Deardorff (1970) and Schumann (1975) in early large-eddy simulation (LES) studies, and continue to be used at present for both direct simulation (Gavrilakis 1992) and LES.

The cases under study were the ERCOFTAC test case T3a and T3b (Savill 1992, 1993), in which a free-stream turbulence level of 3% or 6% is superimposed on a parallel flow of $U_0 = 9.6m/s$. The free-stream disturbance decays at a known rate (Roach and Brierley 1992), while the transition takes place rapidly underneath it. There is a nominally zero pressure gradient since the boundary layer growth was compensated in the experiments.

Transition of the flat-plate boundary layer in the presence of free-stream turbulence

(f.s.t.) has been investigated for both 3% to 6% u'/U at the leading edge. A true large-eddy simulation (LES) was carried out using a subgrid-scale model similar to that of Smagorinsky (1963) and Lilly (1967),

$$\nu_s = (\Delta c_s)^2 \sqrt{2 s_{ij} s_{ij}}, \tag{1}$$

modified as described by Voke (1990),

$$\nu_e = \nu_s - \frac{2\nu}{n}[1 - \exp(-n\nu_s/2\nu)], \tag{2}$$

to allow for low-Reynolds-number effects. The constant c_s was set to 0.1, and $n = 9$. The subgrid model was found to be almost inactive in the laminar region very close to the wall, but had some influence on the behaviour of the free-stream turbulence and on the boundary layer in and downstream of transition.

2.2 Mesh resolution

The LES of transition under 6% f.s.t. was performed in a computational box extending from $Re_x = 6620$ to $Re_x = 200000$, or a total nominal length of 300mm, equivalent to $L_x^+ = 10138$ in wall units. The lateral and vertical dimensions of the box were $L_z = 20$mm ($L_z^+ = 676$) and $L_y = 30$mm ($L_y^+ = 1014$), and the overall meshing was $127 \times 56 \times 48$. These dimensions gave a resolution $\Delta_x^+ = 80$, $\Delta_z^+ = 14$, and Δ_y^+ varying from 1 at the wall to 80 well beyond the boundary layer. The wall units are based on the friction velocity just after transition is complete.

The other simulations were performed without the subgrid scale model, though the resolution was not sufficiently high in any case to justify calling them fully resolved or direct. The fine simulation, also with 6% f.s.t. at inflow, was performed in a computational box of twice the length used for the LES ($L_x = 600$mm, $L_x^+ = 20317$) but the same lateral and vertical dimensions. The meshing was $255 \times 56 \times 48$, so that the grid resolution was identical to that used for the LES. The coarse mesh simulations referred to later were performed in the double length box, with vertical and lateral box sizes unchanged, and meshing of $255 \times 32x \times 16$, giving $\Delta_x^+ = 80$, $\Delta_z^+ = 42$, and Δ_y^+ varying from 1.4 to 122. Two simulations using 3% and 6% f.s.t. were carried out at this resolution, and the numerical experiments discussed in section 3.2 were also carried out at the same resolution. The time steps were $\Delta t^+ = \Delta t u_\tau^2/\nu = 0.1656$ for the fine mesh simulation and the LES, and $\Delta t^+ = 0.3325$ for the coarse simulations. The Courant numbers in all simulations were maintained below 0.25 and the viscous numbers were around 0.15.

The geometry of the computations is sketched in Figure 1, and the details of the various runs and numerical experiments are summarised in Table 1. For comparison with Roach and Brierley (1992) and other published work on these test problems,

	LES	Fine	Coarse
L_x	300mm	600mm	600mm
L_y	30mm	30mm	30mm
L_z	20mm	20mm	20mm
L_x^+	10138	20317	20317
L_y^+	1014	1014	1014
L_z^+	676	676	676
N_x	127	255	255
N_y	56	56	32
N_z	48	48	16
Δ_x	2.35mm	2.35mm	2.35mm
Δ_z	.417mm	.417mm	1.25mm
Δ_x^+	80	80	80
Δ_y^+	1–80	1–80	1.4–122
Δ_z^+	14	14	42

Table 1: Meshing of the simulations

it is convenient to use the dimensional units mm and m/s and hence time units of ms. The relationship between these units and the nominal viscous units, which are based on the friction at a position just downstream of transition, is defined by

$$u_\tau = 0.49\text{m/s} \tag{3}$$

$$\nu = 0.0145\text{mm}^2/\text{ms} \tag{4}$$

Thus 1mm $= 33.79\nu/u_\tau$ and 1ms $= 16.56\nu/u_\tau^2$. Reynolds numbers may also be deduced using the above value of ν and $U_0 = 9.6$m/s. Our results are given at four x stations, at 25mm, 45mm, 95mm and 195mm, at which $Re_x = 16600$, 29800, 62900, 129100 respectively.

2.3 Boundary conditions

The upstream boundary of the computation represented a point 10mm downstream of the leading edge of the flat plate ($Re_x = 6620$). We imposed an appropriate Blasius profile at the inflow boundary, with the free-stream disturbances limited to the region above $y = 0.3$mm. There was a smooth cutoff of free-stream disturbances between $y = 0.3$mm and $y = 0.65$mm. The inflowing f.s.t. was derived from separate simulations (Figure 1) on matched meshes but without any solid lower surface, and with pseudorandom disturbances at their inflow superimposed on a uniform flow. Velocity data were extracted from these simulations at $x = 150$mm, 50mm upstream of the outflow boundary of the simulations. These 'precursor' simulations therefore mimicked the behaviour of grid turbulence, generating more realistic f.s.t. for input into the simulation of the boundary layer transition than the pseudorandom input

f.s.t. used by Yang and Voke (1992). The pseudorandom disturbances at the inflow of the precursor simulations decayed rapidly at first, but settled to a more physically realistic decay rate before they reached the $x = 150$mm station at which velocity data were extracted for use as inflow to the boundary layer 'successor' simulations.

The inflowing free-stream turbulence for the successor simulations was therefore close to isotropic ($u' : v' : w' = 1 : 1.1 : 0.93$) and was assumed to have most of the required properties of grid turbulence. The deviation from isotropy of the inflowing f.s.t. arose from the anisotropic grid used in the precursor simulations, and did not have a physical significance. The decay of the free-stream turbulence level in the successor simulation occured in line with expectations, Figure 2, after an initial length of slightly faster decay left over from the history in the precursor simulations. The figure shows that the presence of the sub-grid scale model resulted in a slightly faster decay of the free-stream turbulence.

The outflow boundaries were treated by the simple advective method proposed by Potamitis and Voke (1992). The outflow was well downstream of the main region of interest which extended up to and through transition. At the outflow, the boundary layer thickness $\delta_{99}^{+} = 446$ (in the worst case) was about 44% of the box height. A steady and uniform outflow of $0.00625U_0$ was imposed through the upper boundaries in the fine simulation and LES to compensate for the boundary layer growth; the mean pressure gradient in these simulations was therefore very close to zero.

The LES was initiated by taking the upstream half of the fine mesh simulation after 300ms, inserting the subgrid-scale model, and simulating for a further 400ms. The detailed statistics to be presented later were gathered between 40ms and 400ms after the subgrid-scale model was switched on.

3 Results

3.1 Transition

The simulation predictions are compared with two appropriate sets of experimental results (Roach and Brierley 1992) at 3% and 6% f.s.t. Transition was found to occur in positions in broad agreement with available experimental data, as judged by the change in friction factor, Figure 3, or shape factor, Figure 4. The transition occurred early, about a sixth of the way down the longer box in the 6% f.s.t. case, and the resolution of the mesh appears not to have had a major influence on the position of transition. The presence of the subgrid-scale model caused a slightly early start to transition, a long transition, and a slower approach to the turbulent level of wall friction. Figures 5 and 6, showing the relationship between friction coefficient and shape factor and Re_ϑ, compare our LES with various experimental data. The LES

appears to predict the later part of transition in a more convincing manner than the other simulations, implying that the subgrid model played a useful rôle where real turbulence was present. The transition started early but developed slowly in the LES, a tendency apparent to a lesser extent in the other simulations as compared with the experimental data.

The mean profiles from the LES, Figure 7, clearly indicate the change from a laminar to a turbulent character occurring through transition. The agreement with the experiment of Roach and Brierley is good. The other simulations gave a similar picture.

Figures 8, 9 and 10 show the r.m.s. fluctuation profiles for the LES at the same positions, and again the agreement is generally good, particularly for u' where the experimental data is also most reliable. The experimental data for v' and w' unfortunately is not available nearer to the wall. The peaks seen in the intensities, broadly at the correct position and with the correct magnitude, indicate that the LES captures the essential fluid dynamics occurring in the laminar layer prior to transition, and give considerable confidence that the true physical processes of bypass transition are being reproduced numerically. Again the other simulations gave a similar picture.

Figure 11 shows the profiles of the principal Reynolds stress $\overline{u'v'}$ at $x = 45$mm and $x = 95$mm. The predictions are clearly high relative to the data; unfortunately it is easy to underestimate $\overline{u'v'}$ in hot-wire measurements by misorienting the probe slightly, and some doubt has been cast on the validity of the experimental data. Since we have no reason to excuse our predictions, it would be very useful to have further information on the true level of the stress.

Figure 12 shows a view of u' as a function of x and y (stretched), graphically displaying the early transition. Figure 13 is a similar representation of the ratios between the grid spacings Δy and Δz and the dissipation (Kolmogorov) length scale

$$l_k = (\nu^3/\epsilon)^{1/4}. \tag{5}$$

It is apparent that the y resolution close to the wall, which is dictated more by the requirement to accurately represent the high gradients there, is more than adequate in terms of the disipation scale; the grid scale is in fact less than l_k. In the free stream, the ratio δ_y/l_k reaches 20 while Δ_z/l_k varies between 3 and 12.

3.2 Numerical experiments

The presence of the pre-transition peaks in the simulation results gave us confidence that the mechanisms of transition were being broadly reproduced by the numerical simulations even at the low resolutions used. In an attempt to elucidate the mechanisms at work in producing these fluctuations in the laminar layer and the early transition, a number of numerical experiments were carried out, based in every case on the 6% f.s.t. level and using the coarse mesh. Such simulations were cheap and fast to perform, and gave rapid pointers to the principal physical mechanisms involved. The numerical experiments were:

1. Disturbances were introduced directly into the laminar layer in place of free stream turbulence.
2. Fluctuations other than u' were omitted from the inflow turbulence.
3. Fluctuations other than v' were omitted from the inflow turbulence.
4. Fluctuations other than w' were omitted from the inflow turbulence.
5. There was no inflow free stream turbulence at all.
6. Inflow turbulence was present above $y = 5$mm only.
7. Inflow turbulence was present above $y = 10$mm only.
8. No wall damping of the inflow turbulence was imposed.
9. A layer of high viscosity was inserted between $y = 4.13$mm and $y = 7.7$mm, with inflow turbulence above $y = 7.7$mm only.
10. The inflow turbulence was tagged with a temperature marker above 7.7mm.

The form and results of each of these numerical experiments will be described in turn.

3.2.1 Disturbances inside the layer

We find that disturbances introduced directly inside the laminar boundary layer at the inflow are ineffective in provoking transition in the absence of f.s.t., unless the disturbance levels are very high. Such disturbances are generally damped rapidly by viscosity and the presence of the wall, with the layer settling back into an undisturbed laminar profile and continuing downstream without undergoing transition. Very high levels of disturbance inside the layer at the inflow, on the other hand, could provoke an immediate and dramatic transition.

3.2.2 Anisotropic f.s.t. at inflow

In each of the next three numerical experiments, two components of the disturbances transferred from the precursor simulation were omitted on the inflow plane only of the boundary layer simulation. The nonzero component was taken from the precursor simulation of decaying grid turbulence, but the other two components were omitted from the inflow boundary specification. The Navier-Stokes approximation which is solved in the body of the simulation quickly started to redistribute energy among the components, and so the energy was not restricted to one component for long. In spite of this, the behaviours in the three cases were quite different and revealing.

The results are shown in Figure 14. It is immediately clear that the presence of the u' component at the inlet plane had little importance in the triggering of the bypass transition. The most important component was v', which triggered transition exactly as if the full isotropic disturbance were present. w' triggered transition late, though this may be because of redistribution of energy into the v' component downstream of the inflow plane. These tests confirmed the importance of wall-normal disturbances in bypass transition, known from the experiments of Kachanov *et al.* (1978).

3.2.3 No f.s.t. disturbance

The test with no f.s.t. or other disturbances confirmed that the laminar layer was stable. There was no sign of T.S. waves or other incipient stages of transition.

3.2.4 Inflow f.s.t. restricted to above 5 or 10mm

It was found that transition occurred early when the f.s.t. fluctuations were removed from the laminar layer and the region near the wall, and were restricted to the part of the inflow boundary well into the free stream. Only when the inflow f.s.t. was removed from a region adjacent to the wall of thickness comparable to the length scale of the f.s.t. did the transition move downstream, Figure 15. This confirms that it is the direct interaction of the f.s.t. with the layer that produces the pre-transition peaks and the early transition.

3.2.5 Inflow turbulence without imposed wall damping

This test allowed us to confirm that the damping of the f.s.t. v' component imposed in the main simulations was similar to that found when the unmodified f.s.t.

encountered the wall in the numerical test, Figure 16. A further related test was carried out because of concern that the form of the inflow boundary condition was triggering the transition. In the main simulations, the inflow plane was 10mm downstream of the nominal leading edge of the plate, since the finite-volume simulations could not resolve the very thin boundary layer close to the leading edge. However, the u' disturbances appeared in the layers very early, within a few mesh cells of the inflow plane: it was therefore considered important to verify that the same type of transition occurred when the inflow boundary was removed from any direct contact with the laminar layer. A test with the inflow 20mm upstream of the leading edge, and no imposed wall damping, gave results almost identical to the first of these two tests.

3.2.6 Viscous slab

The numerical experiment with a highly viscous layer was performed to verify the hypothesis that inviscid pressure-mediated action plays an important role in transferring disturbances into the layer at an early stage. Raised viscosity was introduced into a layer between $y = 4.13$mm ($y^+ = 118.3$) and $y = 7.7$mm ($y^+ = 223.43$); it was not associated with moving fluid. The viscosity in the slab was raised to 100 times the normal molecular viscosity of air. The disturbances on the inflow plane were again approximately isotropic with $u' = v' = w' = 6\%$ but were limited to the region beyond the viscous slab. Figure 17 shows that the position of transition was hardly affected by the presence of the viscous layer suggesting that irrotational motions induced by the pressure field, interacting with the strong shear of the laminar layer, were sufficient to provoke the behaviour normally seen. The pre-transition peaks were found to be present in this test. The test indicated that the length scale of the f.s.t. is crucial to the dynamics, since motions on this scale could jump the viscous slab without difficulty.

3.2.7 Temperature tagging

Tagging the f.s.t. with a passive tracer (nominally a raised temperature, though no buoyancy effects were allowed) confirmed that transition took place when the tagged free-stream fluid came into contact with the laminar shear, Figure 18.

3.3 Damping functions

The large-eddy simulation has been used to study the behaviour of ratios which enter commonly-used $k-\epsilon$ closure models as damping functions. The damping function f_μ enters the definition of the turbulent eddy viscosity for such closures,

$$\nu_t = C_\mu f_\mu \frac{k^2}{\epsilon}. \tag{6}$$

Here $C_\mu = 0.09$ is constant and ϵ is the dissipation. All the quantities in (6) could be computed directly from the simulation, using any suitable components of mean stress and strain to obtain the eddy viscosity required. We used only the principal component of stress, so that the simulation predicted the form of the damping function as

$$f_\mu(x,y) = -\frac{\overline{u'v'}\,\epsilon}{\overline{\partial u/\partial y}\,C_\mu\,k^2}. \tag{7}$$

We compare this damping function with those used in three closure models that have been used to predict bypass transition. In the model of Launder and Sharma (1974) the function f_μ is estimated as

$$f_\mu = \exp[-3.4/(1 + k^2/50\nu\hat{\epsilon})^2], \tag{8}$$

where

$$\hat{\epsilon} = \epsilon - 2\nu(\partial\sqrt{k}/\partial y)^2. \tag{9}$$

The modified dissipation $\hat{\epsilon}$ is also used in (6) when computing the turbulent eddy viscosity with this model. The model of Lam and Bremhorst (1981) uses

$$f_\mu = [1 - \exp(-0.0165y^*)]^2(1 + 20.5k^2/\nu\epsilon). \tag{10}$$

The model of Chien (1982) has simply

$$f_\mu = 1 - \exp(-0.0115u_\tau y/\nu). \tag{11}$$

but like the Launder-Sharma model uses a modified disspation function in (6) when computing the turbulent eddy viscosity, though in this case the form is

$$\tilde{\epsilon} = \epsilon - 2\nu k/y^2. \tag{12}$$

The nondimensional coordinates occurring in these models, $y^+ = u_\tau y/\nu$ and $y^* = \sqrt{k}y/\nu$ are readily computed in the simulation together with the modified dissipations, allowing the forms of the model damping functions to be compared with the LES predictions. The models for f_μ are used in (6) each with the appropriate dissipation function ($\hat{\epsilon}$ for Launder-Sharma or $\tilde{\epsilon}$ for Chien; Lam-Bremhorst uses ϵ unmodified) so for each model we have used a consistent version of the simulation damping function computed from (7) with the appropriate modified dissipation in place of ϵ.

Figure 19 shows the damping functions (simulated and modelled) for the three models, as a function of y at the positions $x = 25, 45, 95, 195$mm. The results are different from those presented by Yang and Voke (1993) since we have improved our method of extracting ϵ from the LES since those results were obtained. (Appendix A, section A.11 gives details of the old and new methods of obtaining ϵ.) It is now clear that the model of Launder and Sharma has a general form for the wall damping closer to the true picture than originally thought, which may acoount for its success in predicting this type of transition (Savill 1992). Further work is proceeding, aimed at determining the best nondimensional variables to use for describing the damping through transition.

3.4 The mechanisms of transition

In the light of the numerical experiments, we concluded that the normal component of f.s.t. is crucial in the receptivity of the boundary layer, which is provoked into transition by exposure to free-stream v' in continuing interaction with the laminar shear. A check of the profiles of v' and $\partial U/\partial y$ at various upstream stations, Figure 20, confirmed that there was a region where both were non-zero. The shape of the v' profile is partly determined by a damping imposed on the f.s.t. intensity profiles at the inflow plane; by comparing the profile at an early station with that output from the numerical experiment performed without any imposed damping, Figure 21, we confirm that the profile is physically realistic.

Further insight depended on a full analysis of the balance equations for several components of the Reynolds stress. This was performed for the LES, the results being gathered from a database of 800 samples extending over a simulation period $t^+ = 6600$. The methods we used for extracting the balance terms are described in detail in Appendix A.

Figure 22 shows the balance of the principal stress $\overline{u'v'}$ at the four stations $x = 25, 45, 95, 195$mm. The residual error term $\overline{\partial_t(u'v')}$, arising from lack of statistical convergence, was significant at some stations, but in these cases was clearly associated with an equal and opposite deviation in the convection term. In all other equations where the error term was nonzero (it was generally much smaller than in the case in Figure 22) an association with a deviation of the convection term from expectations was also suspected: we therefore combined the error term into the convection for all the data. Other terms arising from the existence of a subgrid eddy viscosity in this simulation were so much smaller than those shown that they could be safely omitted.

Figure 23 is the balance of $\overline{u'v'}$ with the error absorbed. We see that the production is balanced by a combination of the other terms. In Figure 24 the hypothesis that the production of $\overline{u'v'}$ arises from the interation of f.s.t. v' with the laminar shear is

confirmed. So, although $\overline{v'^2}$ is strongly damped and a closer look at the v' balance reveals that there is an extremely low level of production of $\overline{v'^2}$ in the layer, the early $\overline{u'v'}$ production is driven by the overlap between the f.s.t. and the mean laminar shear. The resulting production of $\overline{u'v'}$ is balanced by convection, pressure, turbulent transport and viscous terms, with equal importance. The resulting turbulence stress should be correlated with the externally imposed v', and strongly concentrated into the second and fourth quadrants.

The balance of $\overline{u'^2}$ is shown in Figure 25, and with the statistical error absorbed in Figure 26. Inspection of the terms contributing to the production of $\overline{u'^2}$ has confirmed that the $-\overline{u'v'}dU/dy$ term is much larger than any other, as demonstrated in Figure 27: the peak in $\overline{u'^2}$ is therefore consequential on the peak in $\overline{u'v'}$. The growth in the peaks occurs though the slowly increasing overlap between dU/dy (as the laminar boundary layer grows) and the wall-normal f.s.t. fluctuation v' (which does not change its damped y profile but decays slowly in x with the f.s.t. level). This interaction therefore takes place between two essentially independent phenomena.

Figure 28 shows the $\overline{v'^2}$ balance, and Figure 29 the same terms with the statistical error absorbed. It is immediately apparent that v' within the layer behaves quite differently from u' and is totally distinct from the f.s.t. v'. Production is negligible at all stations, and the redistribution of u' motions into v' does not take place immediately: there is no evidence of a redistribution that responds to the u' production in a simple way. The pressure term eventually makes itself felt, resulting in the appearance of the v' peak in transition. No other terms contribute to this peak. Figures 30 and 31 show the $\overline{w'^2}$ balance, in the same style as previous figures. The dynamics of w' are broadly similar to that seen for v', though in this case the damping effect of the wall has less influence. Again the pressure term is the source of the peak that appears in transition.

A simple, intuitive, and physically credible picture emerges from our analysis of the stress balances from the LES. The f.s.t. v' field, damped by the resisting pressure field generated in response to the presence of a wall, overlaps with the high mean shear of the laminar layer to an extent that is dictated by the ratio of the f.s.t. length scale and the boundary layer thickness. In the region of overlap a high $\overline{u'v'}$ production is present, balanced by diffusive, convective, and dissipative actions. This in turn generates a high $\overline{u'^2}$ production, again balanced by a mixture of actions. This first stage of boundary layer receptivity is an external action of the f.s.t. wall-normal fluctuating field on the high shear, lifting low-speed fluid away from the wall and pushing high-speed fluid towards it, generating a fluctuating u' layer that is a pure response to the external v'. Because of the high level of shear in the boundary layer, the u' generated can be larger than the f.s.t u' or v': the high shear acts as an amplifier of fluctuations, as well as converting external v motions into boundary-layer u motions.

How can a peak of $\overline{u'v'}$ coexist with a very low level of $\overline{v'^2}$ production and no peak in $\overline{v'^2}$? This source of confusion is important to clarify: the peak in the $\overline{u'v'}$ is exclusively a correlation between the free-stream v' and the wall-layer u' . There is *no* correlation between u' and v' in the f.s.t., nor is there yet a wall-layer component of v'. We see that the distinction between the two types of turbulence is essential to an understanding of turbulence generation in the layer. It is also evident that the dynamics is essentially anisotropic, since the rôles of u' and v' are quite different. Any approach that combines the fluctuation components, as in simple closure models that use k as a measure of turbulence activity, is at a severe disadvantage. It is hard to see how such a model can capture the physical dynamics described above; only a second moment closure has any hope of modelling the distinct rôles of u' and v'. Furthermore, the f.s.t. and boundary-layer turbulence may need to be modelled separately, and the influence of the f.s.t. length scale be recognised in the modelling.

The second stage of the boundary layer receptivity is less clear. It is evident that the first stage does *not* immediately give rise to redistribution of fluctuating energy into the v' and w' components; instead we see a buildup of u' through convection in combination with continued stage-1 production of u'. It would be useful to understand why the pressure redistribution is delayed. The previous figures showing balances all include a total pressure term comprised of both pressure diffusion and pressure-strain. The separation of each pressure term into its two parts gives rise to further statistical and interpolation errors (see section A.10), but the definition we have used is natural and gives convincingly smooth curves as well as enforcing the condition that the sum of the pressure-strain terms for $\overline{u'^2}, \overline{v'^2}$ and $\overline{w'^2}$ must equal zero.

Figure 32 shows these three pressure-strain terms. We see that the separation of the pressure term into pressure strain and pressure diffusion does little to clarify the dynamics; in the case of the v'^2 balance, near the wall the pressure strain is negative during and after transition, and is offset by an approximately opposite pressure diffusion, so that there is a redistribution from both u' and v' into w'. We presume that the redistribution from u' is a response to the high level of u'^2, while that from v' must arise from the resistance offered by the nearby wall to v motion, which gives rise to fluctuating pressure gradients that oppose the v' diffusing from further out.

Further from the wall we see the more natural situation of u' being redistributed into v' and w'. This we understand, though it is still a mystery why the pressure dynamics changes so rapidly between x =45 and 95mm.

4 Conclusions

Large-eddy simulation has been shown to be a viable approach for the study of transition under turbulence. Numerical experiments have been performed showing the importance of the normal component of the free stream turbulence in stimulating bypass transition. Computations of damping functions used in several popular closure models highlight likely problems in reconciling the models with our simulated dynamics.

Evidence from the balance equations derived directly from our LES supports the importance of wall-normal free-stream disturbances. The wall-normal component of the f.s.t. is damped in the presence of the wall in a manner determined by the f.s.t. length scale alone, prior to transition. The overlap between the f.s.t. v' profile and the large shear in the layer sets the level of production of fluctuating shear stress, and this in turn leads to production of streamwise disturbances inside the layer. The redistribution of u' into the other components is delayed, its onset coinciding with the start of transition in the zero-pressure-gradient case we have studied. The reasons for the delay of pressure redistribution are not yet understood, and are the subject of current research and discussion.

5 Acknowledgements

This work was carried out under grant GR/H 24556 from the U.K. Science and Engineering Research Council and Rolls Royce plc, whose support we gratefully acknowledge. The technical advice from Profs Brian Launder and Peter Stow and Drs Mark Savill and John Coupland is particularly appreciated.

6 References

Bryan, K. (1966). 'A Scheme for Numerical Integration of the Equations of Motion on an Irregular Grid Free of Nonlinear Instability'. *Monthly Weather Review*, **94**, pp 39–40.

Chien, K-Y. (1982). 'Predictions of Channel and Boundary-Layer Flows with a Low Reynolds Number Turbulence Model'. *AIAA J.*, **20**, 33–38.

Coles, D.E. (1962). 'The Turbulent Boundary-Layer in a Compressible Fluid'. *Rand. Rep. R403-PR, ARC 24473*: Appendix A: A Manual of Experimental Practice for Low-Speed Flow.

Deardorff, J.W. (1970). 'A numerical study of three-dimensional turbulent channel flow at large Reynolds numbers'. *J. Fluid Mech.*, **41**, pp 453–480 .

Erm, L.P., Smith, A.J., and Joubert, P.N. (1985). 'Low Reynolds Number Turbulent Boundary Layers on a Smooth Flat Surface in a Zero Pressure Gradient'. *Proc. 5th Symp. on Turbulent Shear Flows*, Ithaca, N.Y.

Fasel, H. (1976). 'Investigation of stability of boundary layers by a finite-difference model of the Navier-Stokes equations'. *J. Fluid Mech.*, **78**, 335–383.

Fasel, H., Rist, U., and Konzelmann, U. (1990). 'Numerical Investigation of the Three-Dimensional Development in Boundary-Layer Transition'. *AIAA J.*, **28**, 29–37.

Gavrilakis, S. (1992). 'Numerical simulation of low-Reynolds-number turbulent flow through a square duct'. *J. Fluid Mech.* /bf 244, 101–129.

Kachanov, S., Kozlov, V.V. and Levchenko, V.V. (1978). 'Occurrence of Tollmien-Schlichting Waves in the Boundary-Layer under the Effects of External Perturbations', *Izv. Akad. Nauk S.S.S.R. Mekhanika Zhid. i Gaza.* English Translation: *Fluid Dyn.* **13**, 704–711.

Kachanov, Y., Kozlov, V., Levchenko, V., and Ramazanov, M. (1985). 'On the Nature of K-Breakdown of a Laminar Boundary-Layer, New Experimental Data', in *Laminar-Turbulent Transition; IUTAM Symposium, Novosibirsk, USSR, 1984*, ed. V. Kozlov. Springer, Berlin. 61–73.

Klebanoff, P.S., Tidstrom, K.D., and Sargent, L.M. (1962). 'The Three-Dimensional Nature of Boundary-Layer Instability'. *J. Fluid Mech.*, *12*, 1–34.

Kleiser L., and Zang, T.A. (1991). 'Numerical Simulation of Transition in Wall-Bounded Shear Flows'. *Annu. Rev. Fluid Mech.*, **23**, 495–537.

Lam, C.K.G., and Bremhorst, K.A. (1981). 'Modified Form of the $k - \epsilon$ Model for Predicting Wall Turbulence'. *J. Fluids Eng.*, **103**, 456–460.

Launder, B.E., and Sharma, B.I. (1974). 'Application of the Energy-Dissipation Model of Turbulence to the Calculation of Flow Near a Spinning Disk'. *Letters in Heat and Mass Transfer*, **1**, 131–138.

Launder (1993). Private communication.

Laurien, E., and Kleiser, L. (1989). 'Numerical simulation of boundary-layer transition and transition control'. *J. Fluid Mech.*, **199**, 403–440.

Lilly, D.K. (1965). 'On the Computational Stability of Numerical Solutions of Time-Dependent, Non-Linear Geophysical Fluid Dynamics Problems'. *Monthly Weather Review*, **93**, 11–26.

Lilly, D.K. (1967). 'The Representation of Small-Scale Turbulence in Numerical Simulations'. *Proc. IBM Scientific Computing Symposium on Environmental Sciences.* IBM form no. 320-1951, White Plains, New York. 195-209.

Murdock, J.W. (1977). 'A Numerical Study of Nonlinear Effects on Boundary-Layer Stability'. *AIAA J.*, **15**, 1167–1173.

Murdock, J.W. (1986). 'Three-Dimensional Numerical Study of Boundary-Layer Stability'. AIAA-86-0434.

Orszag, S.A. and Patera, A.T. (1983). 'Secondary instability of wall bounded shear flows'. *J. Fluid Mech.*, **112**, 347–385.

Potamitis, S.G. and Voke, P.R. (1992). 'Numerical Simulation of a Plane Wake'. *Report ME-FD/92.04,* Dept. Mech. Eng., University of Surrey, GU2 5XH U.K., 1992.

Rai, M.M., and Moin, P. (1991). 'Direct Numerical Simulation of Transition and Turbulence in a Spatially Evolving Boundary-Layer'. AIAA-91-1607.

Rist, U. and Fasel, H. (1991). 'Spatial Three-Dimensional Simulation of Laminar-Turbulent Transition in a Flat Plate Boundary-Layer'. *Proceedings of Boundary-Layer Transition and Control.* Cambridge, UK. 25.1–25.9.

Roach P.E., and Brierley, D.H. (1992). 'The Influence of a Turbulent Free-Stream on Zero Pressure Gradient Transitional Boundary Layer Development', in *Numerical Simulation of Unsteady Flows and Transition to Turbulence*, ed. O. Pironneau, W. Rodi, I.L. Ryhming, A.M. Savill, and T.V. Truong. C.U.P.: New York. 319–347.

Savill, A.M. (1992). 'A Synthesis of T3 Test Case Predictions', in *Numerical Simulation of Unsteady Flows and Transition to Turbulence*, ed. O. Pironneau, W. Rodi, I.L. Ryhming, A.M. Savill, and T.V. Truong. C.U.P.: New York. 404–442.

Savill, A.M. (1993). 'Further progress in the turbulence modelling of by-pass transition', in *Engineering Turbulence Modelling and Experiments 2*, ed. W. Rodi and F. Martelli. Elsevier Science: Amsterdam. 583–592.

Schumann, U. (1975) 'Subgrid Scale Model for Finite Difference Simulations of Turbulent Flows in Plane Channels and Annuli'. *J. Comput. Phys.*, **18**, 376–401.

Smagorinsky, J. (1963). 'General Circulation Experiments with the Primitive Equa-

tions: Part I, the Basic Experiment'. *Monthly Weather Review*, **91**, 99–164.

Spalart, P.R., and Yang, K.S. (1987). 'Numerical study of ribbon-induced transition in Blasius flow', *J. Fluid Mech.*, **178**, 345–365.

Spalart, P.R. (1993). 'Numerical Study of Transition Induced by Suction Devices'. *Int. Conference on Near-Wall Turbulent Flows*, Tempe, Arizona, 15–17 March 1993.

Voke, P.R. (1990). 'Multiple Mesh Simulation of Turbulent Flow'. *Report QMW EP-1082*, QMW University of London E1 4NS U.K.

Wray, A., and Hussaini, M.Y. (1984). 'Numerical Experiments in Boundary-Layer Stability'. *Proc. Roy. Soc.*, London Series **A 392**, 373–389.

Yang, Z., and Voke, P.R. (1991). 'Numerical Simulation of Transition Under Turbulence'. *Report ME-FD/91.01,* Dept. Mech. Eng., University of Surrey, GU2 5XH U.K.

Yang, Z., and Voke, P.R. (1992). 'Numerical Simulation of Boundary Layer Transition in the Presence of Free Stream Turbulence', in *Numerical Simulation of Unsteady Flows and Transition to Turbulence*, ed. O. Pironneau, W. Rodi, I.L. Ryhming, A.M. Savill, and T.V. Truong. C.U.P.: New York. 398–402.

Yang, Z., and Voke, P.R. (1993). 'Large-Eddy Simulation Studies of Bypass Transition'. in *Engineering Turbulence Modelling and Experiments 2*, ed. W. Rodi and F. Martelli. Elsevier Science: Amsterdam. 603–611.

Zang, T.A., and Hussaini, M.Y. (1987). 'Numerical Simulation of Nonlinear Interactions in Channel and Boundary-Layer Transition', in *Nonlinear Wave Interactions in Fluids*, ed. R.W. Miksad, T.R. Akylas, and T. Herbert. **AMD-87**. New York: ASME. 131–145.

Zang, T.A. and Hussaini, M.Y. (1990). 'Multiple Paths to Subharmonic Laminar Breakdown in a Boundary-Layer'. *Phys. Rev. Lett.*, **64**, 641–644.

A Appendix: Balance equations

A.1 Background

The equations for the Reynolds stress play an important role in closure models, and since our simulations are used increasingly to provide data on the behaviour of the modelled terms, it is important that we can compute these terms reliably.

The Reynolds stress is $\overline{u_i' u_j'}$, where the overbar denotes the time mean and the primes denote fluctuating parts. In this appendix we drop the primes from the fluctuating parts, and use capitals (U, P, S, etc.) for the total instantaneous quantities, so that

$$U_i = \overline{u_i} + u_i. \tag{13}$$

In this notation the Reynolds stress is written $\overline{u_i u_j}$. An equation for the stress is derived by subtracting the equation for $\overline{u_i}$ from the equation for U_i to obtain an equation for u_i, which is then multiplied by u_j. To this is added u_i times the equation for u_j, giving an equation for the evolution of $u_i u_j$ that is symmetric in i and j. For instance for the time derivative term itself,

$$u_i \partial_t u_j + u_j \partial_t u_i = \partial_t (u_i u_j). \tag{14}$$

By definition of the time average, this term tends to zero in the mean,

$$\partial_t \overline{u_i u_j} \to 0, \tag{15}$$

as the number of samples tends to infinity. A finite sample will always be used in a real simulation, so we can at best expect the mean of this term to reduce as we increase the sample size. In the following sections the overbar indicating the accumulation of the time average is frequently omitted, the equations being given for the terms that contribute to the sum. Nevertheless, terms that are clearly zero in a full average, such as $\overline{u_i} u_j$, are dropped from the balance.

The addition of the symmetrising term obtained by exchanging i and j subscripts is a common feature affecting every term in the Reynolds stress equations. It is denoted $+ i \leftrightarrow j$, which means that to the preceding term or terms is added a similar term or terms with i and j interchanged.

A.2 Derivation of the balance equation

We take the incompressible momentum conservation equation in the form

$$\partial_t U_i + \partial_k (U_i U_k) + \partial_i P - \nu \partial_k S_{ik} = 0, \tag{16}$$

and write down an equation for the mean immediately,

$$\partial_t \overline{U_i} + \partial_k \overline{U_i U_k} + \partial_i \overline{p} - \nu \partial_k \overline{s}_{ik} = 0. \tag{17}$$

The equation for the fluctuations u_i is found by subtraction:

$$\partial_t u_i + \partial_k (U_i U_k - \overline{U_i U_k}) + \partial_i p - \nu \partial_k s_{ik} = 0. \tag{18}$$

We now proceed as outlined in the previous section, multiplying by u_j and symmetrising the indices i and j, to obtain

$$u_j \partial_t u_i + u_j \partial_k (U_i U_k - \overline{U_i U_k}) + u_j \partial_i p - \nu u_j \partial_k s_{ik} + i \leftrightarrow j = 0. \tag{19}$$

A.3 Splitting the terms

The terms in (19) are normally rearranged in order to obtain a form in which each individual term has a straightforward interpretation in the time average. We can immediately drop the term of the form $u_j \partial_k \overline{U_i U_k}$ since its time mean is zero. The time average of

$$u_j \partial_t u_i + i \leftrightarrow j = \partial_t (u_i u_j) \tag{20}$$

tends to zero, but its computation is useful as an indication of the convergence of the statistics.

Using the definition (13) we now expand the first term in (19). Making use of the incompressible continuity relation for both u_k and $\overline{u_k}$, and dropping the term in $\overline{u_i u_k}$ which does not contribute to the time mean, we obtain

$$u_j \partial_k (\overline{u_i} u_k + u_i \overline{u_k} + u_i u_k) + i \leftrightarrow j = u_j u_k \partial_k \overline{u_i} + i \leftrightarrow j + \overline{u_k} \partial_k (u_i u_j) + \partial_k (u_i u_j u_k). \tag{21}$$

These are the familiar production, convection and turbulent transport terms for the Reynolds stress. In deriving these terms it is important to note the frequent use of the continuity condition and the identity for the derivative of a product, for these very natural analytic procedures do not generalise to the finite-volume form of the equations.

The pressure term is normally rearranged as

$$u_j \partial_i p + i \leftrightarrow j = \partial_i (u_j p) + i \leftrightarrow j - p s_{ij}, \tag{22}$$

once more using the identity for the derivative of a product. The first term is called the pressure diffusion, the second is the pressure strain. The viscous term is similarly rearranged as

$$\begin{aligned} -\nu u_j \partial_k s_{ik} + i \leftrightarrow j &= -\nu u_j \partial^2 u_i + i \leftrightarrow j \\ &= -\nu \partial_k (u_j \partial_k u_i) + i \leftrightarrow j + 2\nu \partial_k u_j \partial_k u_i \\ &= -\nu \partial^2 (u_i u_j) + 2\nu \partial_k u_i \partial_k u_j \end{aligned} \tag{23}$$

The first of these terms is the viscous diffusion of stress; the second is the viscous dissipation, ϵ_{ij}.

The terms contributing to the Reynolds stress balance are summarised as follows:

$u_j u_k \partial_k \overline{u_i} + i \leftrightarrow j$	Production
$\overline{u_k} \partial_k (u_i u_j)$	Convection
$u_k \partial_k (u_i u_j)$	Turbulent transport
$\partial_i (u_j p) + i \leftrightarrow j$	Pressure diffusion
$-p s_{ij}$	Pressure strain
$-\nu \partial^2 (u_i u_j)$	Viscous diffusion
$2\nu \partial_k u_i \partial_k u_j$	Viscous dissipation
$\partial_t (u_i u_j)$	Residual error

A.4 Energy balance

The turbulence kinetic energy k is $u_i u_i/2$, with summation over i, often denoted $u^2/2$. The individual contributions u_1^2, u_2^2 and u_3^2 to k are called the turbulence intensities and are (in the time mean) the diagonal components of the Reynolds stress tensor.

Individual balance equations for each diagonal stress therefore exist and are obtained by setting $i = j$ in the corresponding term of the Reynolds stress balance. With summation over i, we obtain the balance equation for $2k$. In summary, the terms are:

$2u_i u_k \partial_k \overline{u_i}$	Production
$\overline{u_k} \partial k u_i^2$	Convection
$u_k \partial_k u_i^2$	Turbulent transport
$2\partial_i (u_i p)$	Pressure diffusion
$-2p \partial_i u_i$	Pressure strain
$-\nu \partial^2 (u_i^2)$	Viscous diffusion
$2\nu (\partial_k u_i)^2$	Viscous dissipation
$\partial_t (u_i^2)$	Residual error

These terms when accumulated in a time average give the balance for individual intensities if *not* summed over i. (There is summation over k). With summation over i also, and dividing each term by 2, we get the terms of the balance of k. In the latter case the pressure strain obviously vanishes.

Note that the expression $u^2 = u_i u_i$ (summed) is only equal to $2k$ in the mean in the convection term. The turbulence transport involves triple products of fluctuations. The viscous dissipation of k is

$$\epsilon = \epsilon_{ii}/2 = \nu(\partial_k u_i)^2 \tag{24}$$

which is positive definite and represents a drain of energy.

A.5 The triple-step method

The attainment of a balance of terms in equations for Reynolds stress, energy and dissipation depends on the fundamental identity:

$$\overline{a\partial_t b + b\partial_t a} = \overline{\partial_t(ab)}. \tag{25}$$

Unfortunately this elementary mathematical identity fails to generalise to discretised time,

$$a\delta_t b + b\delta_t a = a\frac{b^{n+1} - b^n}{\Delta t} + b\frac{a^{n+1} - a^n}{\Delta t} \neq \delta_t(ab) = \frac{a^{n+1}b^{n+1} - a^n b^n}{\Delta t}, \tag{26}$$

unless the undefined a and b factors are replaced by

$$a^C = \frac{a^{n+1} + a^n}{2} \tag{27}$$

and

$$b^C = \frac{b^{n+1} + b^n}{2}. \tag{28}$$

This method uniquely re-establishes the identity (25) in the form

$$\overline{a^C\delta_t b + b^C\delta_t a} = \overline{\delta_t(ab)}. \tag{29}$$

This quantity will tend towards zero with increasing number of statistical samples N of a stationary process.

The method allows us to create balances of Reynolds stress, turbulence energy and dissipation rate from the simulation variables that are strictly analogous to those derived analytically. For instance, consider the simplest example of the balance for u_i^2. We take the time-discrete equation for the fluctuation velocity u_i,

$$\delta_t u_i = \partial_i p + h_i^A \tag{30}$$

in which no superscript is used for the pressure since it is treated by the method of Gavrilakis (1992), while the remaining terms take an A superscript indicating the explicit Adams formula used in our codes:

$$h_i^A = \frac{3}{2}h_i^n - \frac{1}{2}h_i^{n+1}. \tag{31}$$

h_i is the fluctuating part of H_i,

$$h_i = -\partial_k(U_k U_i - \overline{U_k U_i}) + \nu \partial_k s_{ik}. \tag{32}$$

The equation is multiplied by u_i^C (with no summation over i):

$$u_i^C \delta_t u_i = \delta_t u_i^2 = -u_i^C \partial_i p + u_i^C h_i^A \tag{33}$$

The accumulated time average of this combination must tend toward zero because the time mean of

$$\delta_t u_i^2 = \frac{(u_i^{n+1})^2 - (u_i^n)^2}{\Delta t} \tag{34}$$

tends to zero provided u_i^2 in the simulation does not drift systematically over the period the statistics are accumulated: that is, provided the simulation is statistically stationary.

To compute the terms in $u_i^C h_i^A$, it is necessary to reconstruct the individual parts of h_i at both time steps n and $n-1$ to form part of h_i^A, and multiply it by u_i^C, which requires u_i at steps n and $n+1$. It should be evident that we need

1. mean velocity components and pressure (and temperature in the case of a thermal simulation)
2. fluctuating velocities (and temperatures) at steps $n-1$, n and $n+1$
3. the fluctuating pressure used in moving from step n to step $n+1$.

The velocities (and temperature) are therefore stored at three adjacent time steps and the pressure at one. The means are found first and stored. The data is then scanned, the mean being subtracted to get the fluctuating parts, and the term that is sought is constructed by the product of a C superscript variable with an A superscript combination representing part of the acceleration. This technique has been dubbed the triple-step method for computing terms in balance equations.

A.6 Reynolds stress balance by triple-step

We give the explicit form of the above ideas for the balance of $u_i u_j$. Overbars are omitted.

$$\begin{aligned} \delta_t(u_i u_j) &= u_i^C \delta_t u_j + i \leftrightarrow j \\ &= u_i^C(-\partial_j p + h_j^A) + i \leftrightarrow j \\ &= u_i^C(-\partial_j p - \partial_k(U_k U_j - \overline{U_k U_j})^A + \nu \partial_k s_{jk}^A) + i \leftrightarrow j. \end{aligned} \tag{35}$$

These expressions tend to zero in the limit of sufficiently large and extended samples of a statistically stationary simulation. Exactly as in the analytic derivation of balance equations, the term

$$u_i^C \partial_k \overline{U_k U_j}^A \tag{36}$$

is identically zero, as is the part

$$u_i^C \partial_k \overline{U_k}^A \, \overline{U_j}^A \tag{37}$$

of the triple term. The remaining nonzero terms are:

$u_i^C \partial_k (u_k \overline{u_j})^A + i \leftrightarrow j$	Production
$u_i^C \partial_k (\overline{u_k} u_j)^A + i \leftrightarrow j$	Convection
$u_i^C \partial_k (u_k u_j)^A + i \leftrightarrow j$	Turbulent transport
$u_i^C \partial_j p + i \leftrightarrow j$	Pressure terms
$-\nu u_i^C \partial_k s_{jk}^A + i \leftrightarrow j$	Viscous terms
$\delta_t(u_i u_j)$	Residual error

Note that the pressure and viscous terms are not yet separated into the standard form since the separation depends on details of the spatial discretisation, dealt with below. For the same reasons, the production, mean convection and turbulent transport terms are not rearranged in any way using the continuity equation.

To summarise, the time-discrete balance is computed by the use of a triple-step database obtained from the simulation, which must consist of a sequence of fields at steps $n-1, n$ and $n+1$, allowing the subsequent recomputation of the accelerations used to advance the velocities, and the products of these terms with the combination

$$u_i^C = (u_i^{n+1} + u_i^n)/2. \tag{38}$$

In order to extract the standard production, convection, and turbulent transport terms, it is necessary to recompute the nonlinear terms in three parts, with the velocities being split into mean and fluctuating parts.

A.7 Interpolation and differencing

The triple-step method for balance equations deals with those problems arising from time-stepping in defining a proper balance. It says nothing about the space discretisation, but does imply that the precise forms of spatial interpolation and differencing used to compute accelerations during the simulation should also be used when computing the balance.

The general form of a term in a discrete balance equation using the triple-step method is

$$u_i^C \, a_j + i \leftrightarrow j, \tag{39}$$

where a_j is an acceleration derived exactly as it was during the simulation. For instance in the transport term

$$u_i^C \, \partial_k (u_k u_j)^A + i \leftrightarrow j \tag{40}$$

the second factor must be computed as an Adams term if that scheme is used in the simulation, and the interpolations of u_k and u_j must be exactly the same as those used for U_k and U_j in the simulation. ∂_k must also be the same difference operation used in the simulation. The separation of mean and fluctuating velocity components makes no difference to these requirements. From this point, the notation ∂_k is used to mean the appropriate difference operation rather than an analytic derivative; no ambiguity results from this change.

A.8 Diagonal stresses

For the three cases where $i = j$, the velocity u_i^C and the acceleration a_i are defined at the same point on the staggered mesh (the i face) and the product will naturally be computed there. Thus we compute the balance terms for the diagonal stresses at the same position on the mesh as the diagonal stresses themselves – u_i^2 on the i face and simlarly for hte other two components.

A.9 Off-diagonal stresses

For the off-diagonal stresses, the velocity factor u_i^C and the acceleration factor a_j are defined at different points on the staggered mesh. In spite of this, the balance will be exactly obtained in the limit of a large enough sample when the two factors are interpolated to a common point in a consistent way before being multiplied together.

Suppose we interpolate the velocities u_i^C in the j direction to obtain interpolated velocities denoted v_i^C, and all the acceleration factors a_j consistently in the i direction to obtain interpolated accelerations denoted by b_j. Since the b terms are simple linear combinations of the accelerations actually used in the simulation, they are equal to the time rate of change of the corresponding velocity component u_j, interpolated in the same way in the j direction, denoted w_j.

Thus the sum of all the products will be

$$v_i^C \, \delta_t b_j = (v_i^{n+1} + v_i^n)(w_j^{n+1} - w_j^n)/2\Delta t. \tag{41}$$

We now must add the symmetrising term denoted by $i \leftrightarrow j$. However, the u_i component will still be interpolated in the j direction to obtain v_i, and the u_j component interpolated in the i direction to obtain w_j; thus the symmetrised expression computed must be

$$\begin{aligned} v_i^C \delta_t b_j + i \leftrightarrow j &= [(v_i^{n+1} + v_i^n)(w_j^{n+1} - w_j^n) + (w_j^{n+1} + w_j^n)(v_i^{n+1} - v_i^n)]/2\Delta t \\ &= (v_i^{n+1} w_j^{n+1} - v_i^n w_j^n)/\Delta t \\ &= \delta_t(v_i w_j). \end{aligned} \tag{42}$$

This is exactly what we require: the time rate of change of an off-diagonal stress interpolated to the ij cell edge in any way we choose. Clearly, for consistency with the computed mean off-diagonal stresses and with the simulation dynamics, the interpolation method should be exactly that used for the velocities in the simulation when computing the nonlinear stress terms.

A.10 The pressure terms

The separation of the pressure terms into pressure diffusion and pressure strain (and the similar separation of the viscous terms into viscous diffusion and dissipation) is rather more tricky. The analytic separation,

$$u_i \partial_j p + i \leftrightarrow j = \partial_j(u_i p) + i \leftrightarrow j - p s_{ij}, \tag{43}$$

does not generalise straighforwardly to the discrete representation on a staggered mesh. To do so, u_i and p would have to be defined at the same points in the first term on the right hand side, while u_i on the left hand side (and p in the other term likewise) have to be special unweighted interpolations of these for the identity to hold. None of these requirements can be met easily.

To retain the discretised stress balance, it is vital that the left-hand-side product is computed exactly as the triple-step method demands, namely

$$u_i^C \partial_j p + i \leftrightarrow j \tag{44}$$

The other two terms which we wish to extract must sum to give the left hand side in precisely this form, otherwise the stress equation will no longer balance. The only way to do this is to compute the left hand side product in the way demanded by the triple-step method to give the stress balance, compute separately the pressure strain in a sensible manner at the same point of the staggered mesh, and add the two to obtain the pressure diffusion term.

The computation proceeds as follows. For the diagonal terms, $u_i^C \partial_i p$ is computed at the i face. The pressure strain $2ps_{ii}$ is computed at the cell centre (guaranteeing

that the sum over i will be zero by continuity) and is then interpolated in any way we please to the i face. The diagonal diffusion terms are then computed as

$$2\partial_i(u_i p) = 2u_i\partial_i p + ps_{ii}. \tag{45}$$

The off-diagonal terms $i \neq j$ must be interpolated like the velocities in the nonlinear terms in the simulation, as explained in the previous section, if they are to combine with all the other terms interpolated in the same way to give a stress balance. We proceed as in the previous section to obtain

$$u_i^C\,\partial_j p + i \leftrightarrow j \tag{46}$$

at the ij cell edge. The fluctuating strain rate s_{ij} is also naturally computed at the ij edge. The pressure is interpolated from the centre to this edge in any way we choose, and the off-diagonal diffusion is finally computed as

$$\partial_j(u_i p) + i \leftrightarrow j = u_i\partial_j p + i \leftrightarrow j + 2ps_{ij}. \tag{47}$$

A.11 The viscous terms

The analytic splitting of the viscous term,

$$-\nu u_i\partial_k s_{jk} + i \leftrightarrow j = -\nu u_i\partial^2 u_j + i \leftrightarrow j = -\nu\partial^2(u_i u_j) + 2\nu\partial_k u_i\partial_k u_j, \tag{48}$$

is not easily reproduced on a discrete mesh, for reasons similar to those presented in the case of the pressure rearrangement. Once more, we seek a simple way to ensure that the terms finally output as representing the viscous diffusion and dissipation sum to the expression

$$-\nu u_i^C\,\partial_k s_{jk}^A + i \leftrightarrow j, \tag{49}$$

which must be interpolated in the way described in the preceeding sections in order to guarantee the proper contribution to the overall stress balance. Each diagonal term must be computed on the correct face, and each off-diagonal term at the correct edge.

By analogy with the method proposed for the pressure terms, the sum should be computed in the manner described, with the acceleration $\partial_k s_{jk}^A$ naturally being on the j face, as for the computation of the viscous terms in the simulation. u_i^C is computed on the i face. For the off-diagonal terms the interpolation of the two factors to the ij edge must be done consistently with all the other terms.

The dissipation may now be computed by two-cell central differencing, so that $\partial_k u_i$ is on the i face and $\partial_k u_j$ on the j face. In the case of the off-diagonal terms, the two factors are interpolated to the ij edge in the same manner used for all other terms before being multiplied together. This must be done for all three k values

to obtain the sum over k. The viscous diffusion term is finally computed as the sum. This method was used to compute ϵ for the analysis of damping functions in Yang and Voke (1993). However the dissipation profiles were not convincing, and an alternative method was sought.

On the advice of Launder (1993), the following alternative scheme was tried. The viscous diffusion terms for the diagonal stresses are computed using the discrete Laplacian $\partial^2 u_i^2$ of each squared velocity component, on its own face. The total viscous term is then subtracted to obtain the dissipation:

$$\nu\partial^2(u_i^2) - 2\nu u_i \partial_k s_{ik} = 2\nu(\partial_k u_i)^2 = \epsilon_{ii}. \tag{50}$$

This method has been found to be successful in producing credible profiles of ϵ, which is found by interpolating the three diagonal dissipations ϵ_{ii} to the centre and summing. The method can be extended to the off-diagonal terms, with all interpolations being carried out in the standard manner:

$$\nu\partial^2(u_i u_j) - (\nu u_i \partial_k s_{jk} + i \leftrightarrow j) = 2\nu\partial_k u_i \partial_k u_j = \epsilon_{ij}. \tag{51}$$

B Figures

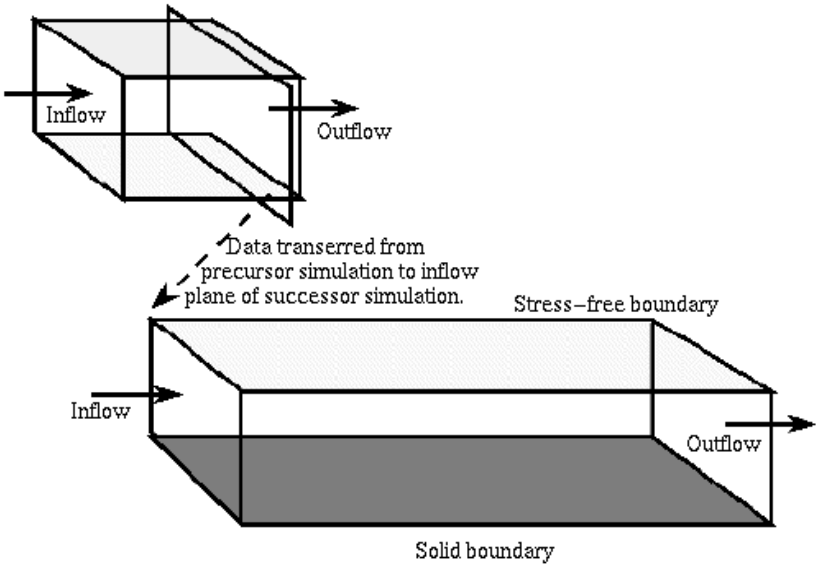

Figure 1. Geometry of the simulations: left, precursor simulation of decaying grid turbulence; right, successor simulation of boundary layer transition under free stream turbulence.

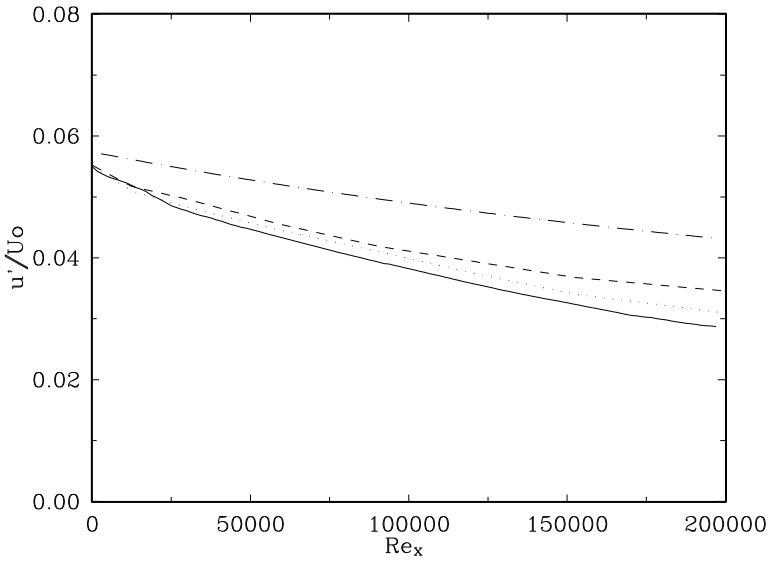

Figure 2. Decay of the free stream turbulence u' in the boundary layer simulation. Solid line, LES; dashed line, fine mesh; dotted line, coarse mesh; chained line, Roach and Brierley (1992).

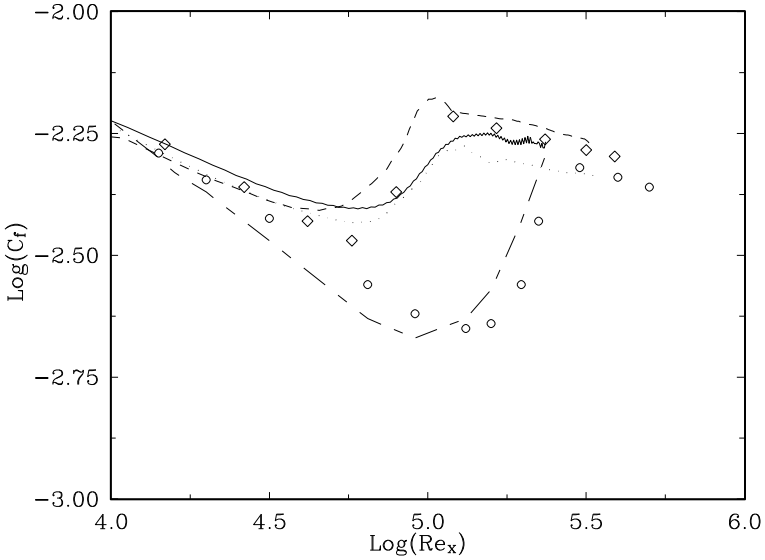

Figure 3. Friction coefficient as a function of Re_x. Solid line, LES, 6% f.s.t.; dashed line, fine mesh; dotted line, coarse mesh; long dashes, coarse mesh simulation with 3% f.s.t.; symbols, Roach and Brierley (1992), 6% or 3% f.s.t.

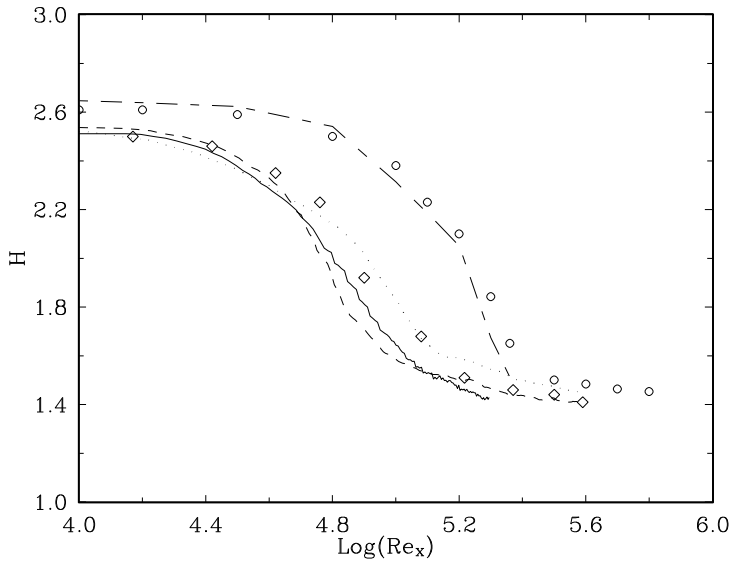

Figure 4. Shape factor as a function of Re_x. As Figure 3.

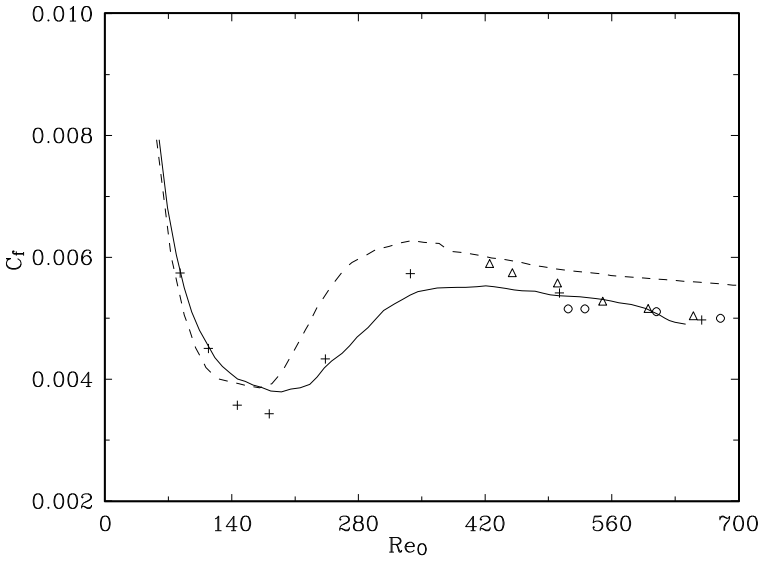

Figure 5. Friction coefficient as a function of Re_ϑ. Solid line, LES; dashed line, fine mesh; crosses, Roach and Brierley (1992); triangles, Coles (1962); circles, Erm *et al.* (1985).

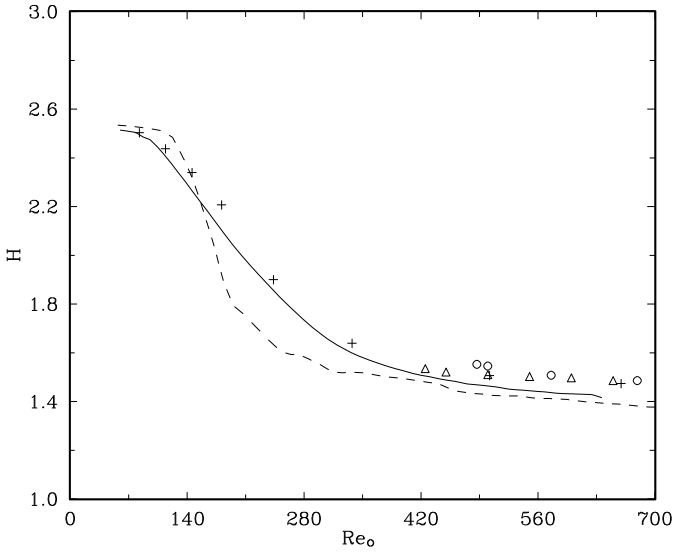

Figure 6. Shape factor as a function of Re_ϑ. As Figure 5.

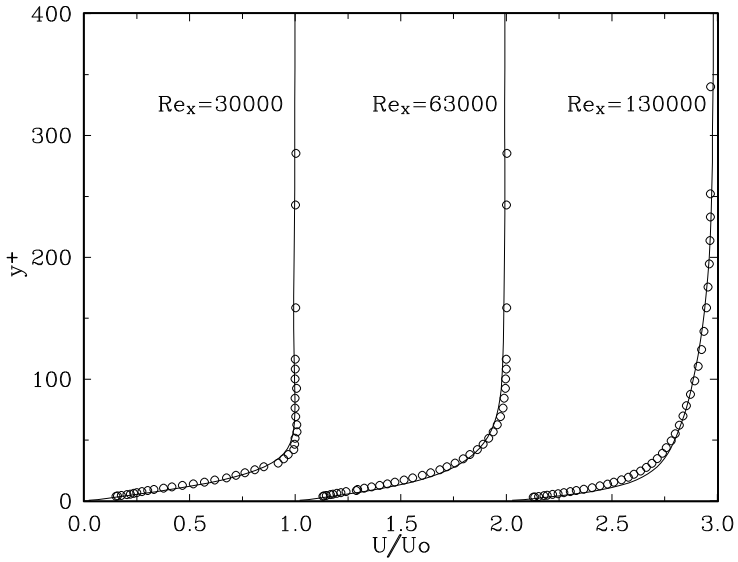

Figure 7. Mean U profiles at three x stations. Solid line, LES; symbols, Roach and Brierley (1992).

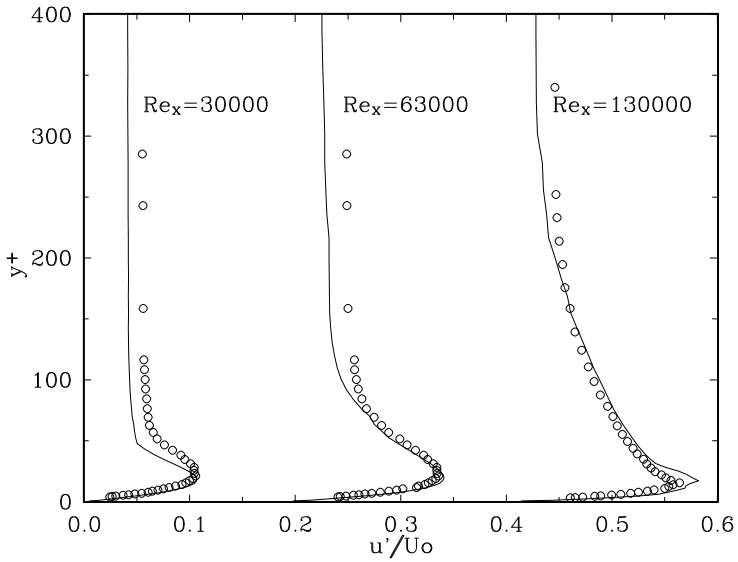

Figure 8. R.m.s. fluctuation u' profiles. As Figure 7.

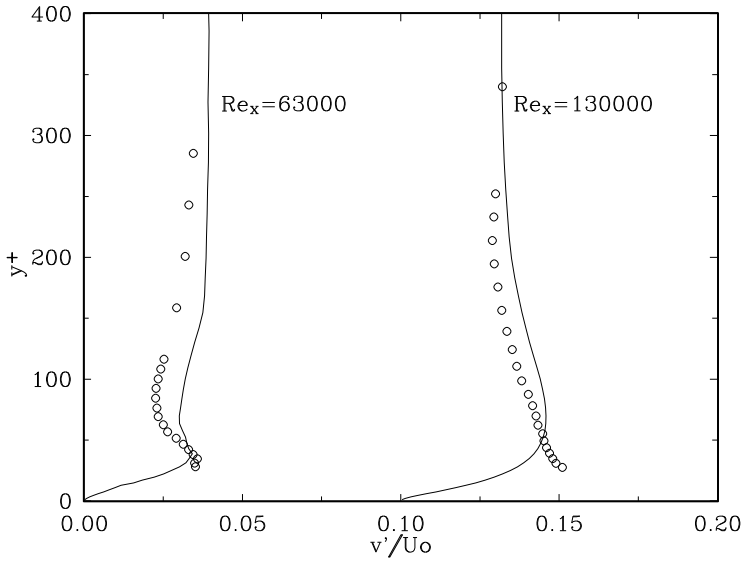

Figure 9. R.m.s. fluctuation v' profiles. As figure 7.

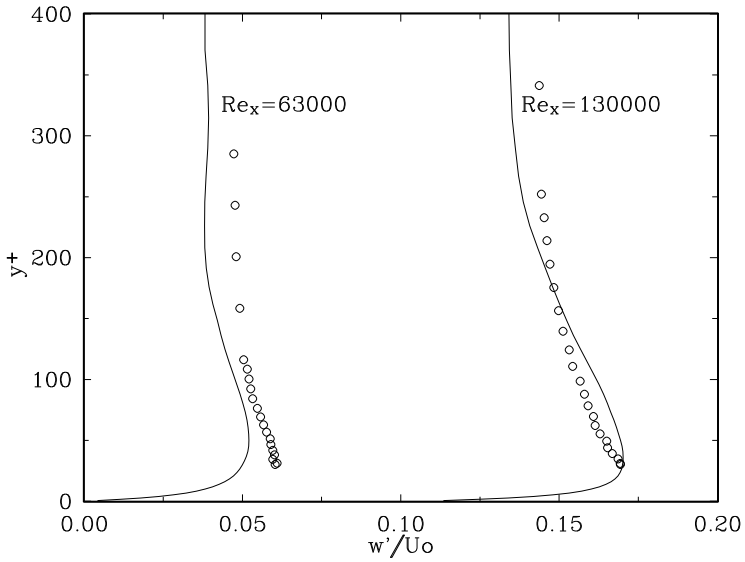

Figure 10. R.m.s. fluctuation w' profiles. As Figure 7.

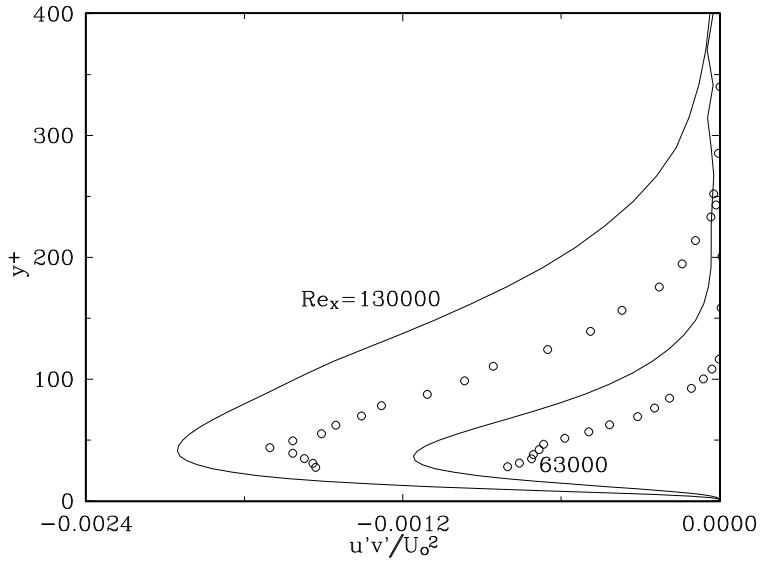

Figure 11. Principal stress $\overline{u'v'}$ profiles. As Figure 7.

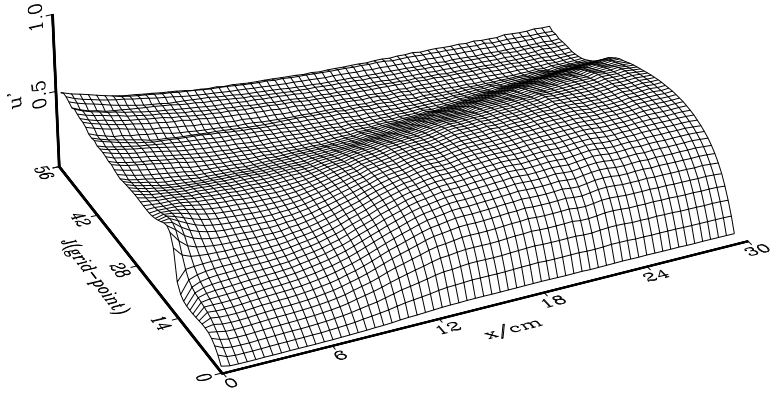

Figure 12. Three-dimensional view of the r.m.s. fluctuation u' distribution in x and J, the wall-normal mesh index.

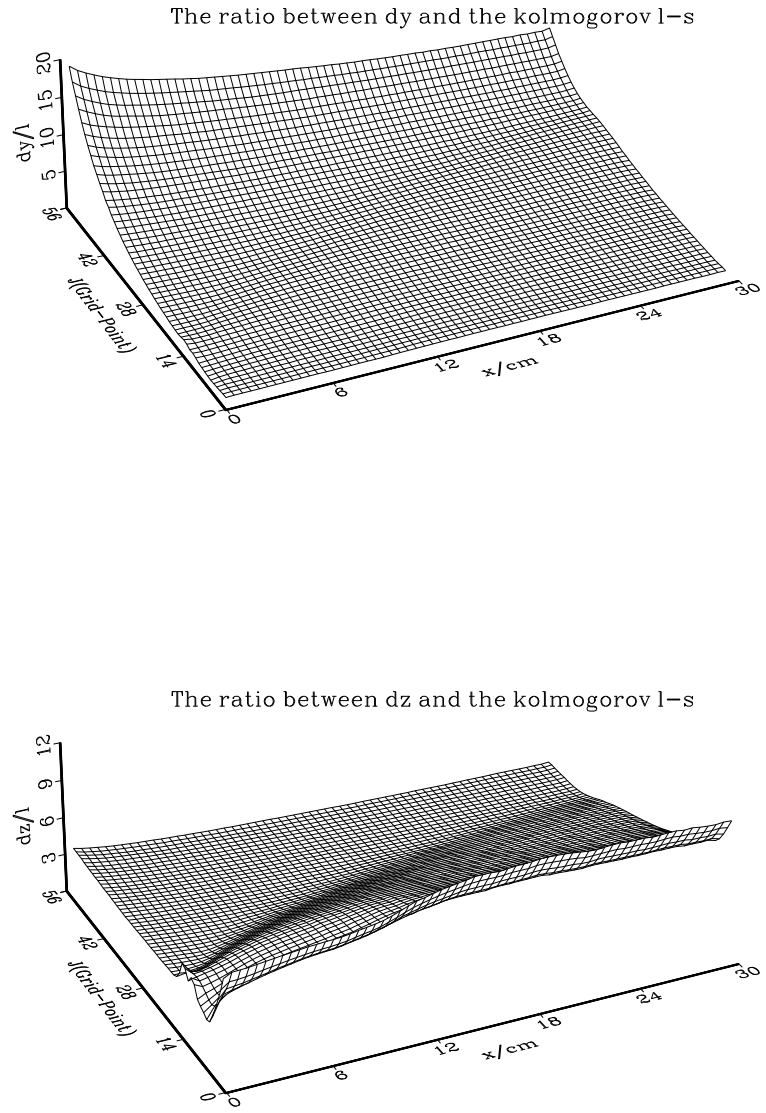

Figure 13. Ratio of mesh size to estimated Kolmogorov length scale. Top, $\Delta y/l_k$; bottom, $\Delta z/l_k$.

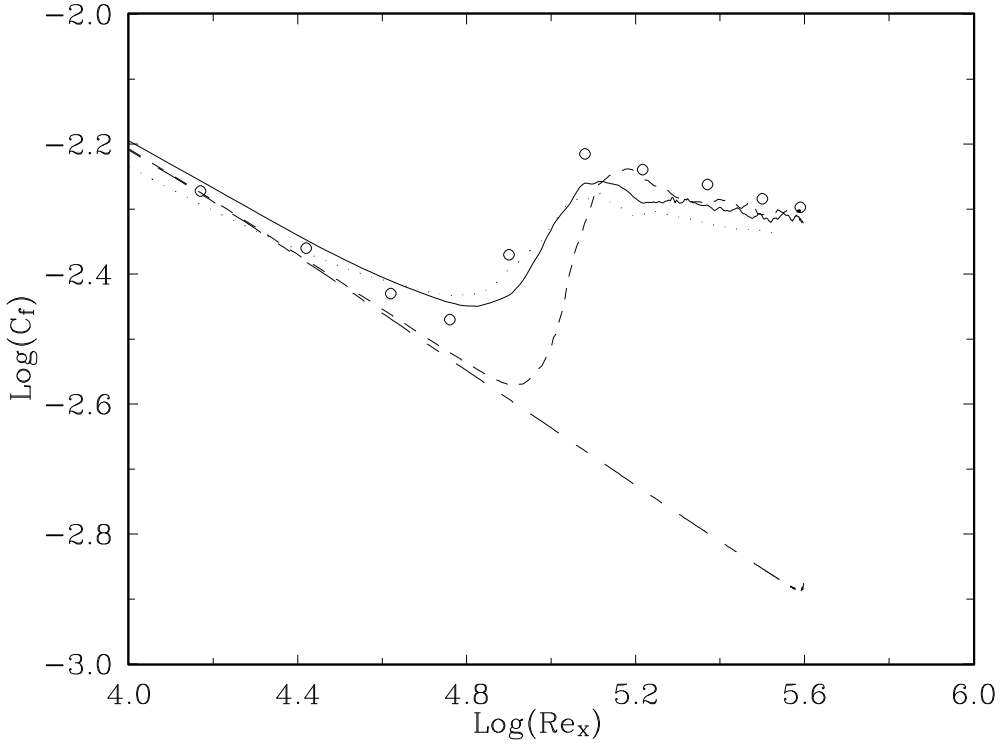

Figure 14. Friction coefficient as a function of Re_x: numerical experiment. Solid line, v' only at inlet; dashed line, w' only at inlet; long dashes, u' only at inlet; dotted line, coarse mesh, normal f.s.t. at inlet; symbols, Roach and Brierley (1992).

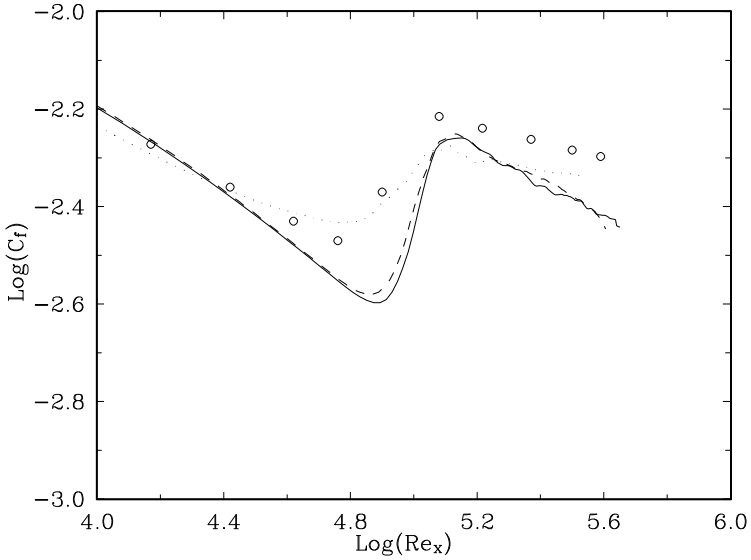

Figure 15. Friction coefficient as a function of Re_x: numerical experiment. Solid line, f.s.t above 10mm at inlet; dashed line, f.s.t. above 5mm at inlet; dotted line, coarse mesh, normal f.s.t. at inlet; symbols, Roach and Brierley (1992).

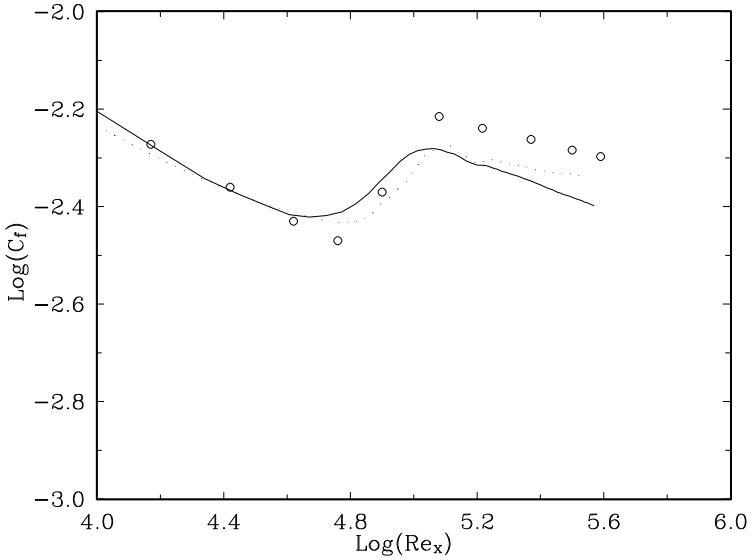

Figure 16. Friction coefficient as a function of Re_x: numerical experiment. Solid line, no damping imposd on f.s.t. at inlet; dotted line, coarse mesh, normal f.s.t. at inlet; symbols, Roach and Brierley (1992).

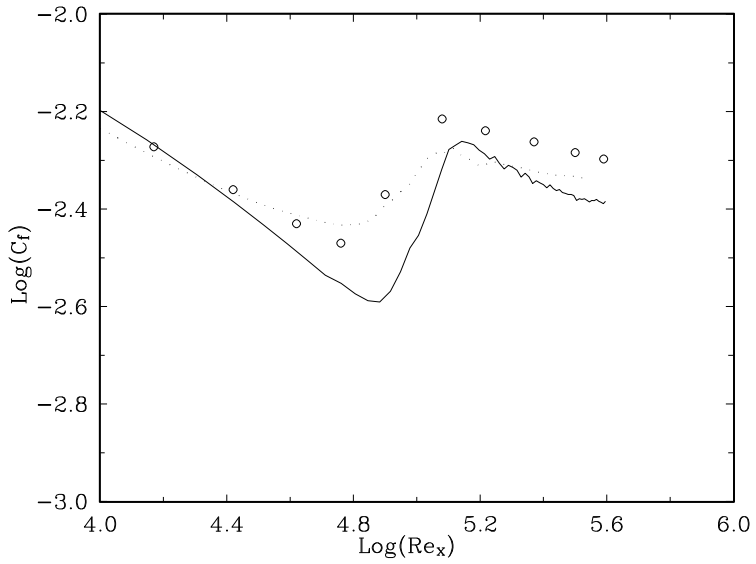

Figure 17. Friction coefficient as a function of Re_x: numerical experiment. Solid line, viscous slab inserted; dotted line, coarse mesh, normal simulation; symbols, Roach and Brierley (1992).

Figure 18. Temperature fluctuation T' in a numerical experiment.

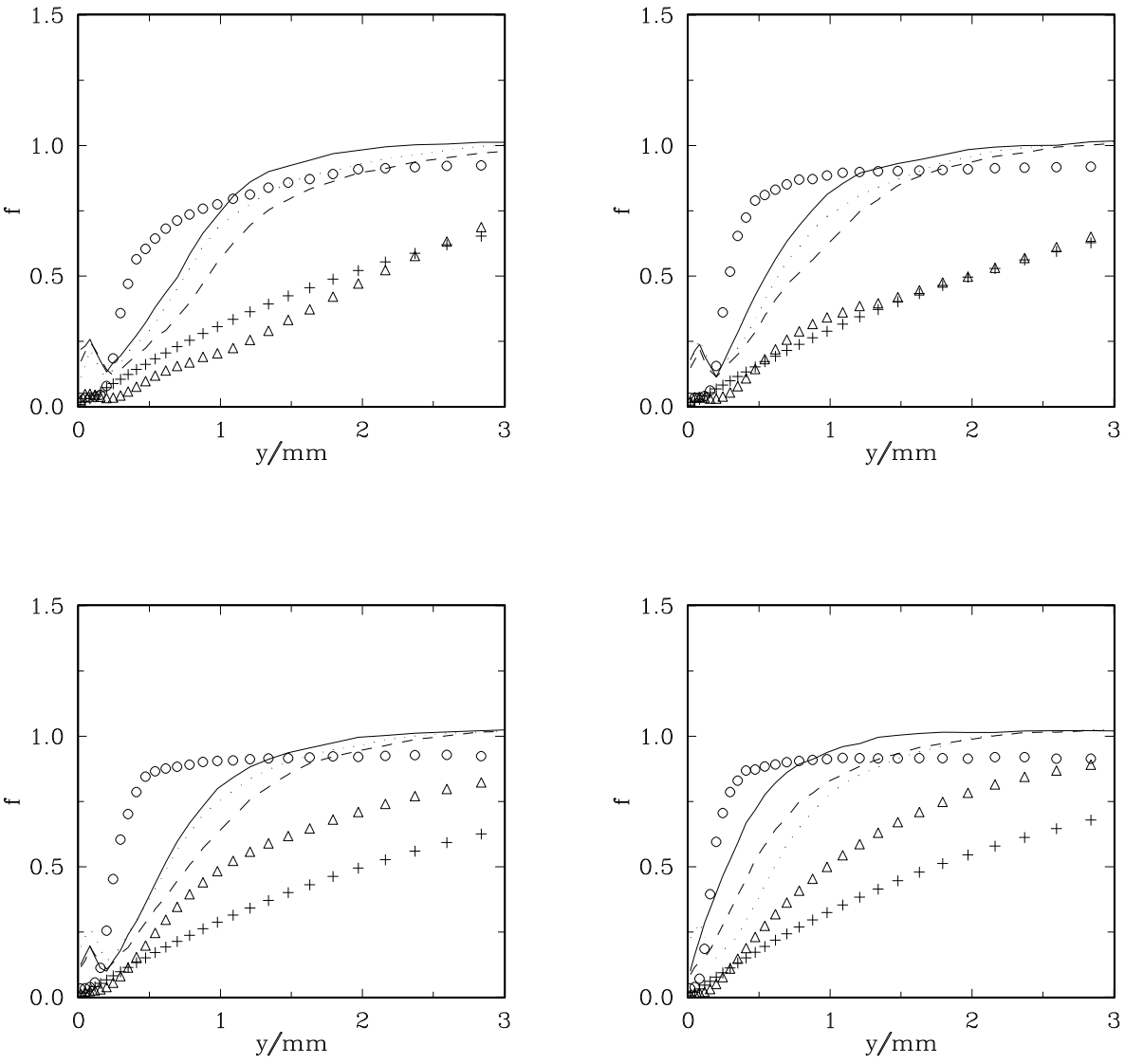

Figure 19. Damping f_μ as functions of y, based on the models of Launder and Sharma (1974), solid line and circles; Lam and Bremhorst (1981), dotted line and triangles; Chien (1982), dashed lined and crosses. Symbols, as predicted by modelling; lines, LES prediction from equation (7). Top left, x = 25mm; top right, x = 45mm; bottom left, x = 95mm; bottom right, x = 195mm.

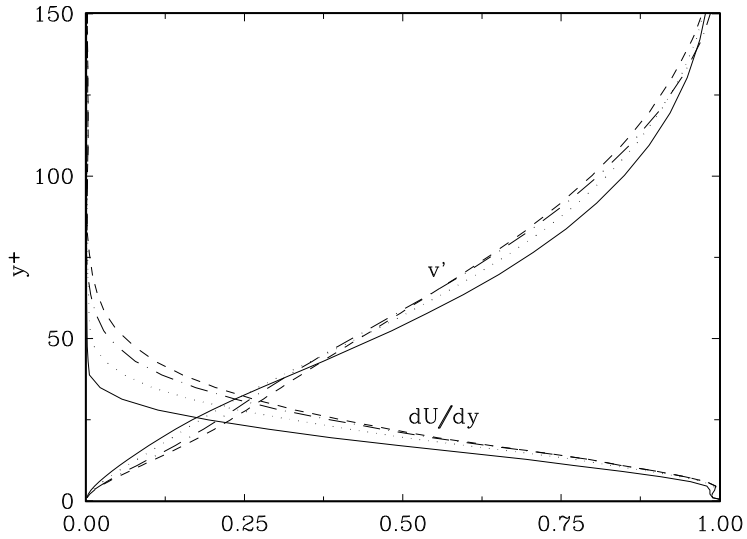

Figure 20. Profiles of r.m.s. fluctuation v' (normalised to the local free-stream value) and principal shear $\partial U/\partial y$ (normalised to the local wall value). solid, 15mm; dotted, 25mm ; chained, 35mm ; dashed, 45mm.

Figure 21. Profiles of r.m.s. fluctuation v' at $x = 15$mm. Solid line, LES, with Blasius profile at inlet and imposed wall damping; dotted, numerical experiment with flat inlet profile and no wall damping.

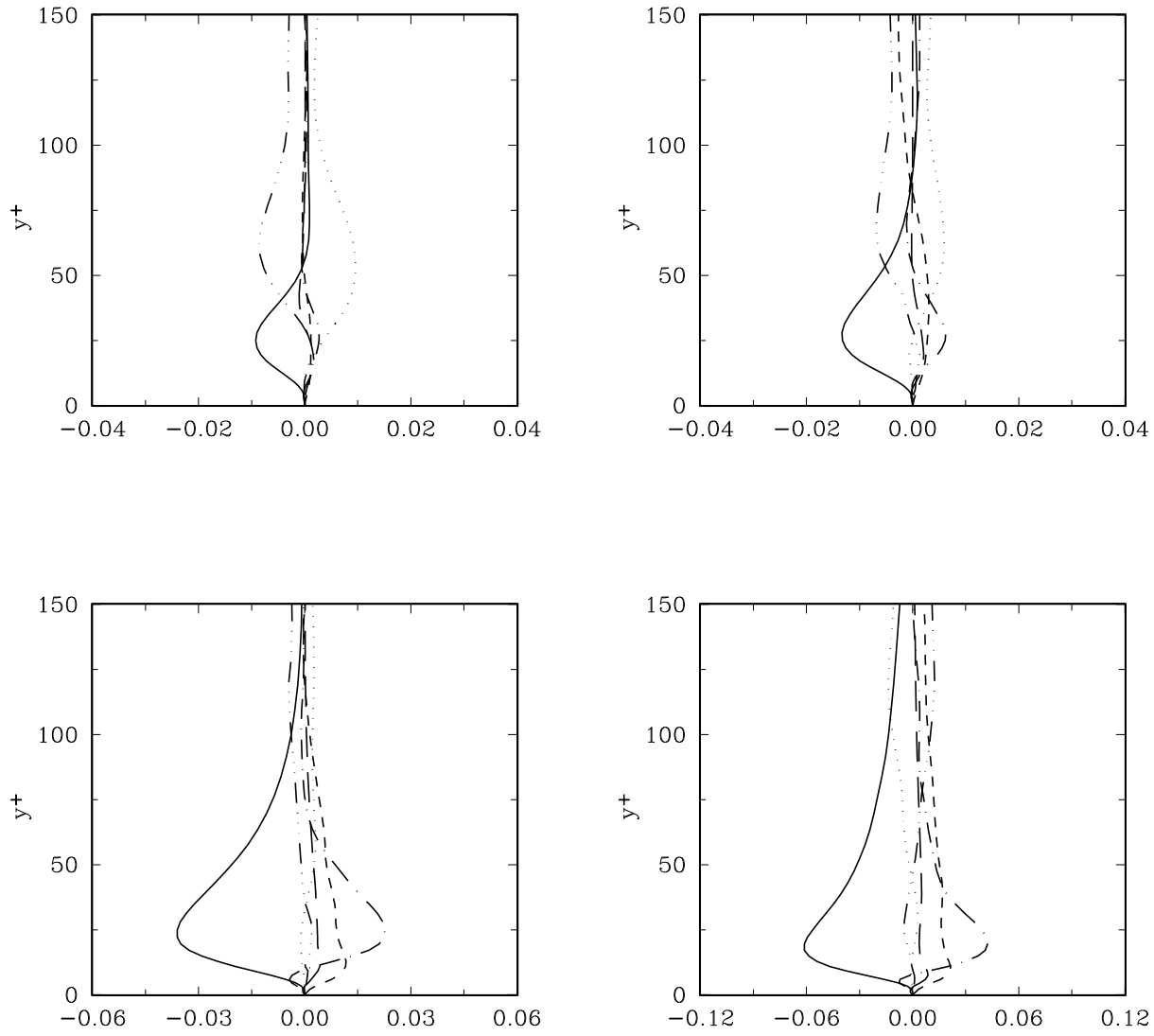

Figure 22. Terms in the balance of $\overline{u'v'}$: Solid line, production; dotted line, convection; dot-dash, turbulent transport; dashed, pressure terms; long dashes, viscous terms; triple-dot-dash, residual error. Top left, $x = 25$mm; top right, $x = 45$mm; bottom left, $x = 95$mm; bottom right, $x = 195$mm.

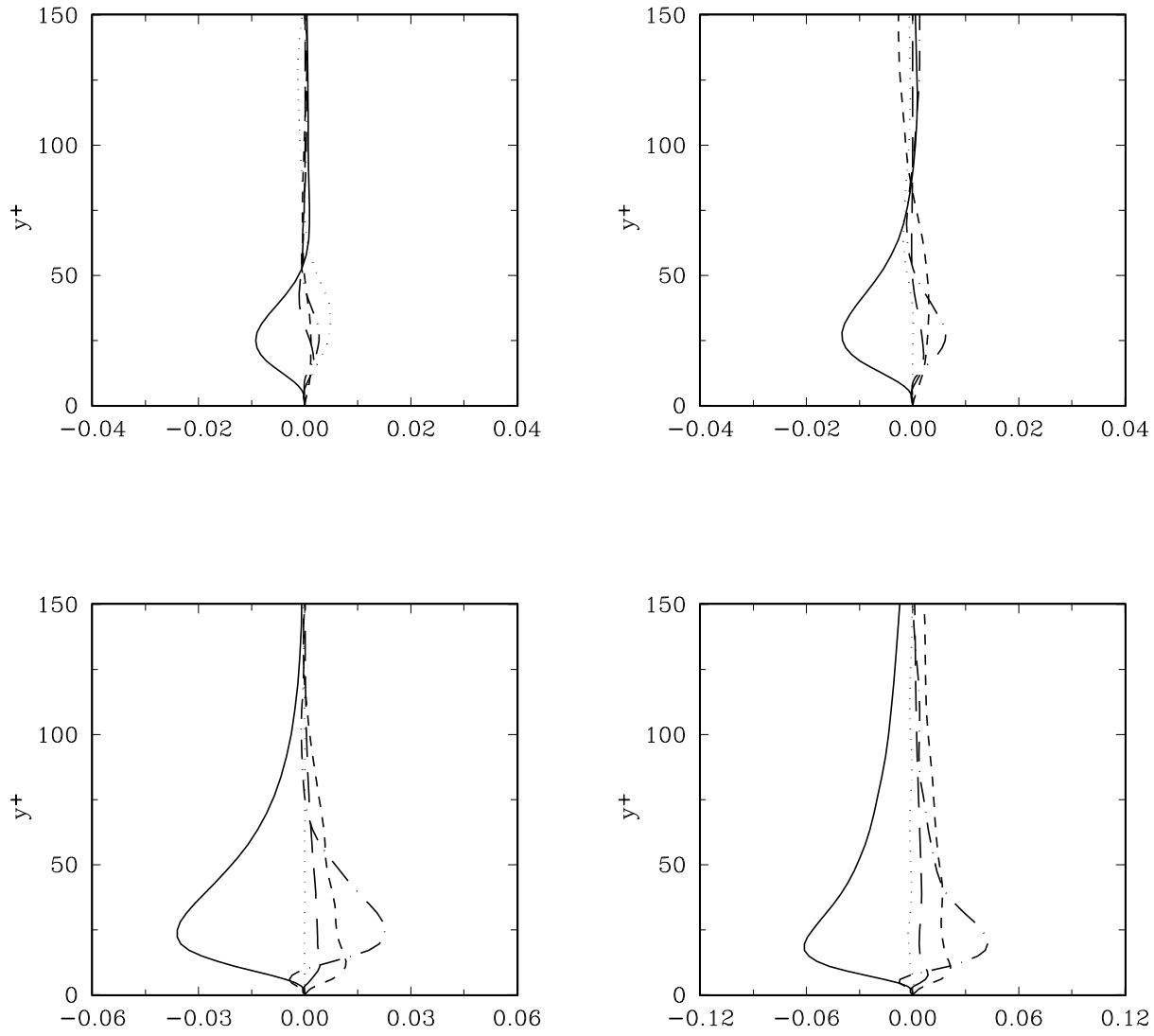

Figure 23. Terms in the balance of $\overline{u'v'}$, with the error term combined with convection. Otherwise, as Figure 22.

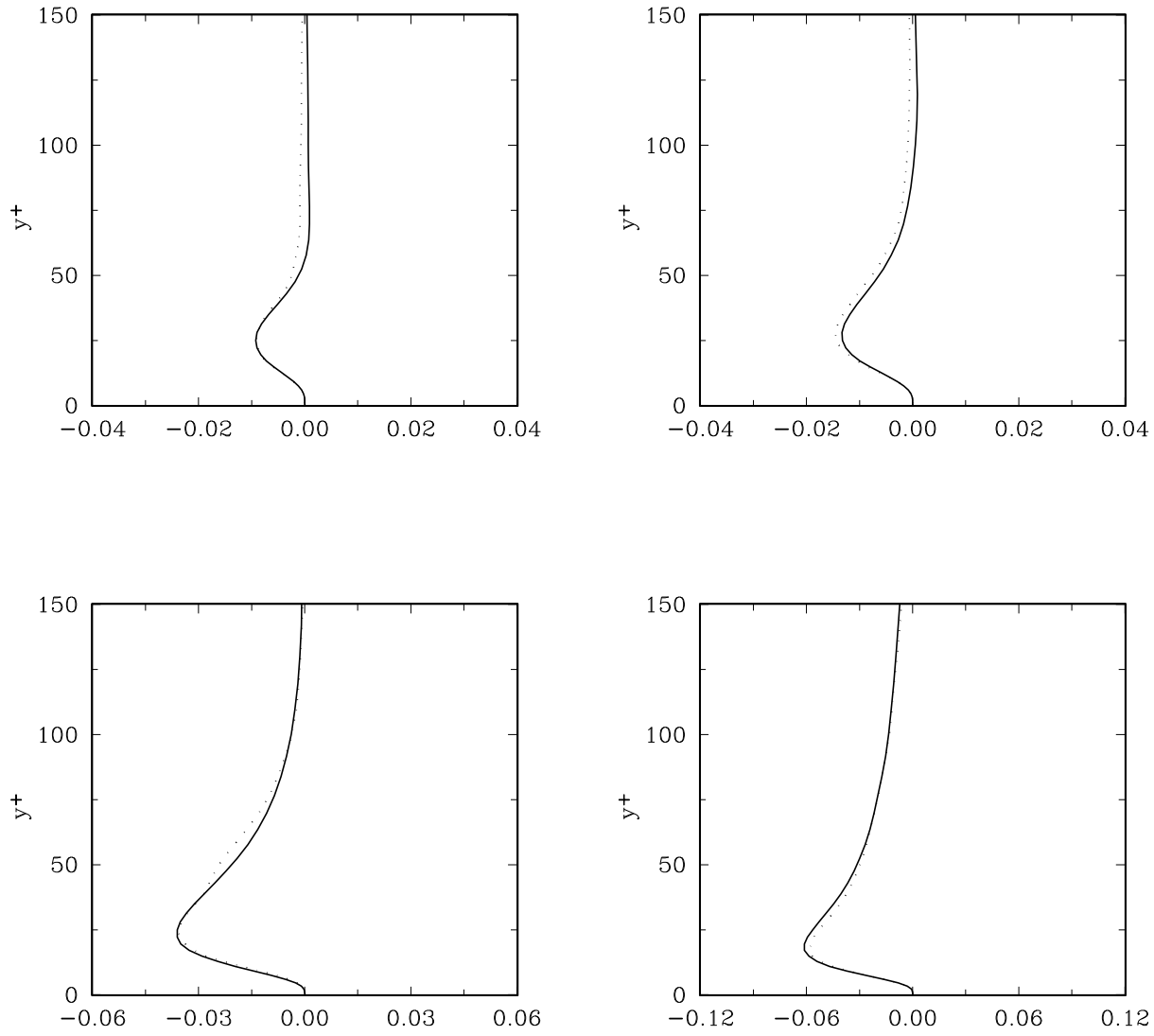

Figure 24. Production terms in the balance of $\overline{u'v'}$. Solid line, total production; dotted line, $-\overline{v'^2}dU/dy$ only.

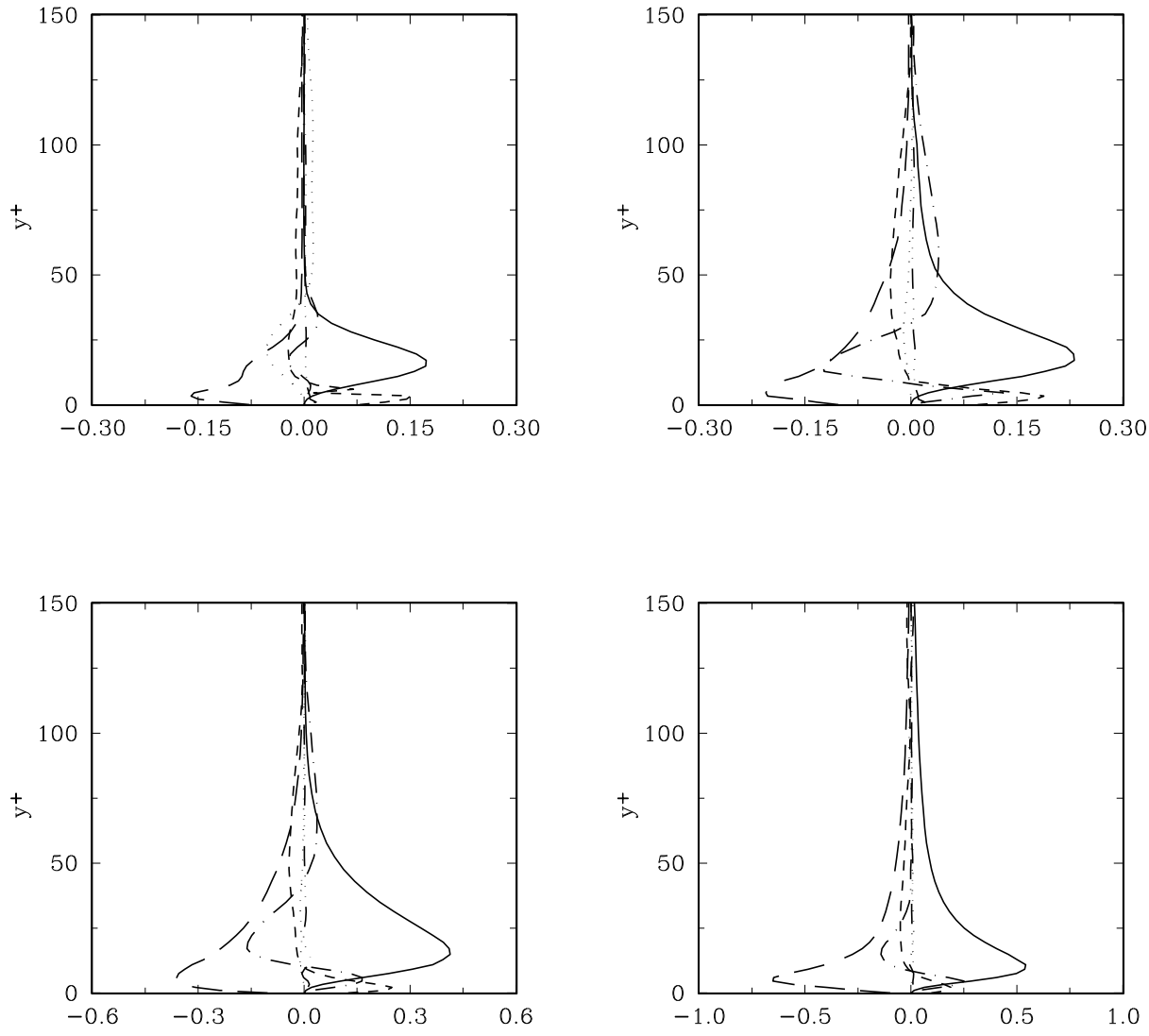

Figure 25. Terms in the balance of $\overline{u'^2}$. As Figure 22.

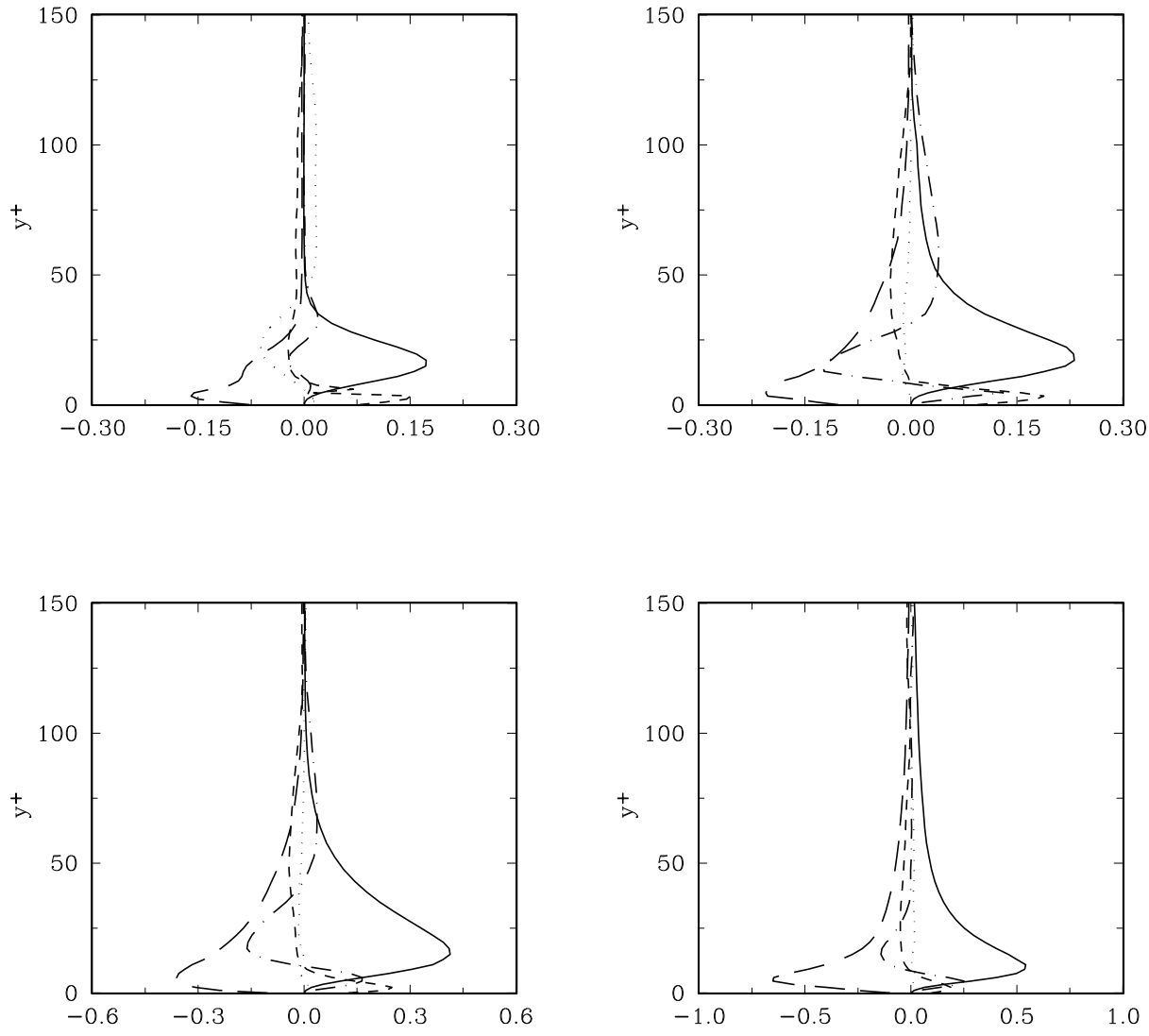

Figure 26. Terms in the balance of $\overline{u'^2}$, with the error term combined with convection. As Figure 23.

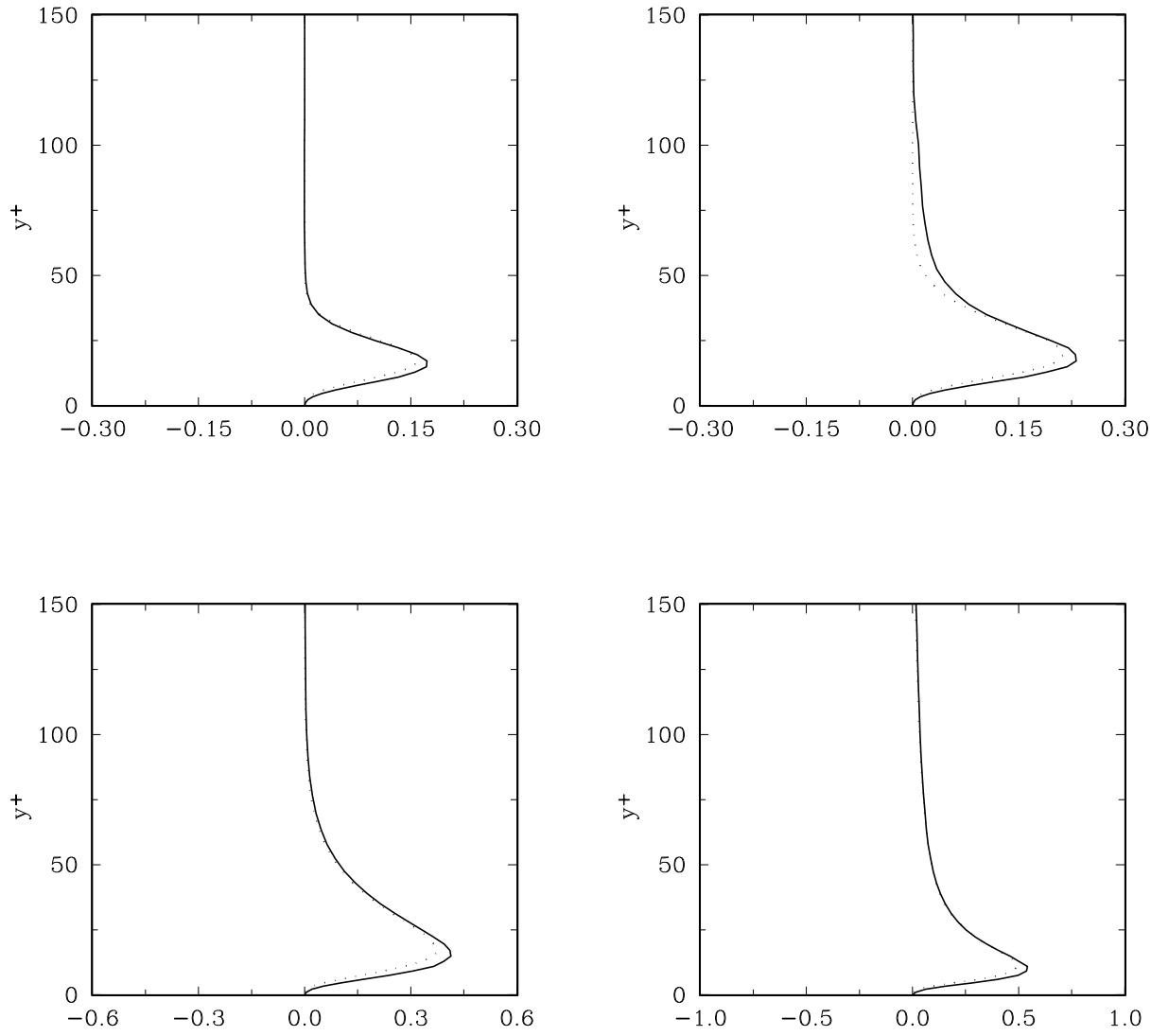

Figure 27. Production terms in the balance of $\overline{u'^2}$. Solid line, total production; dotted line, $-\overline{u'v'}dU/dy$ only.

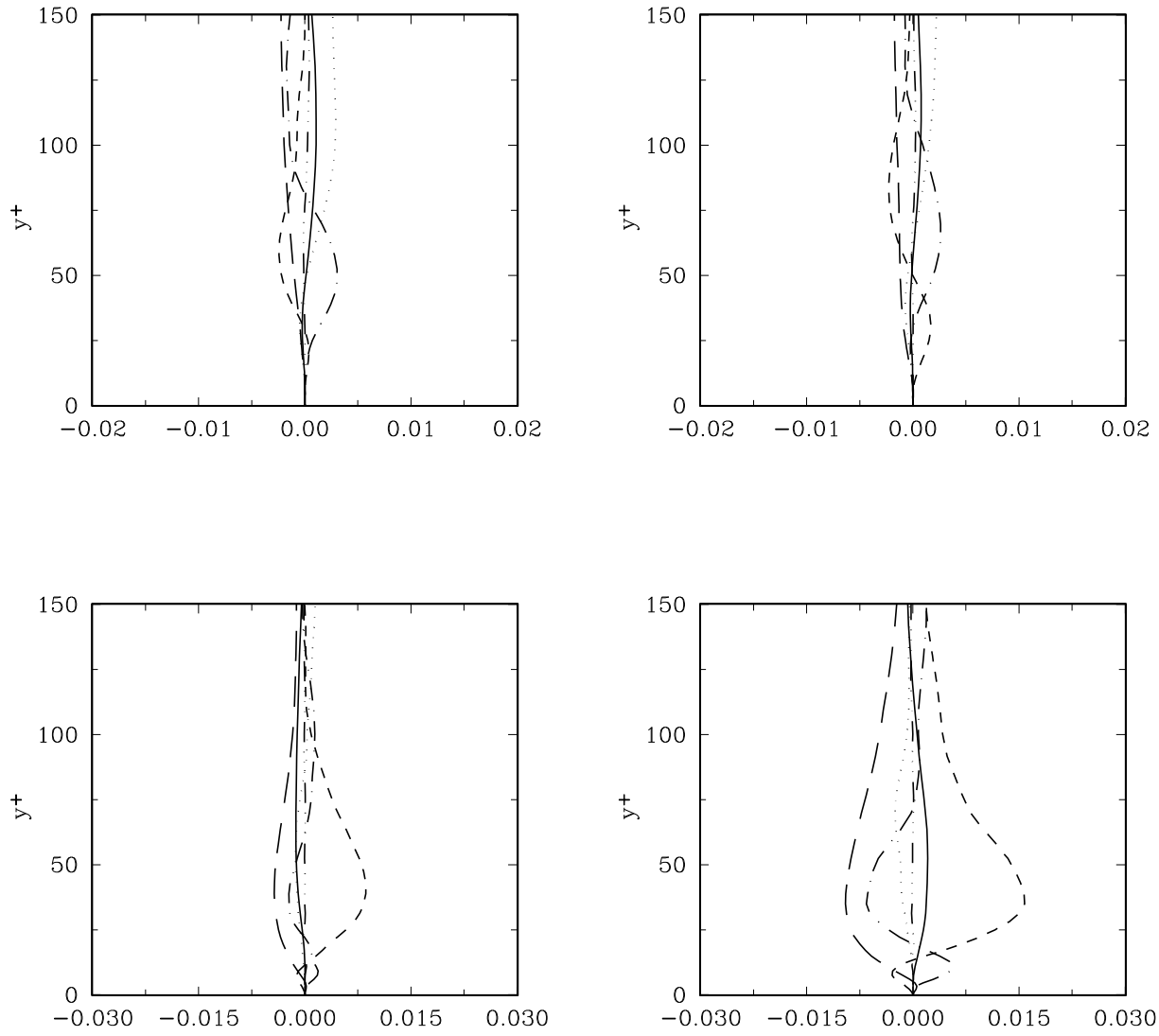

Figure 28. Terms in the balance of $\overline{v'^2}$. As Figure 22.

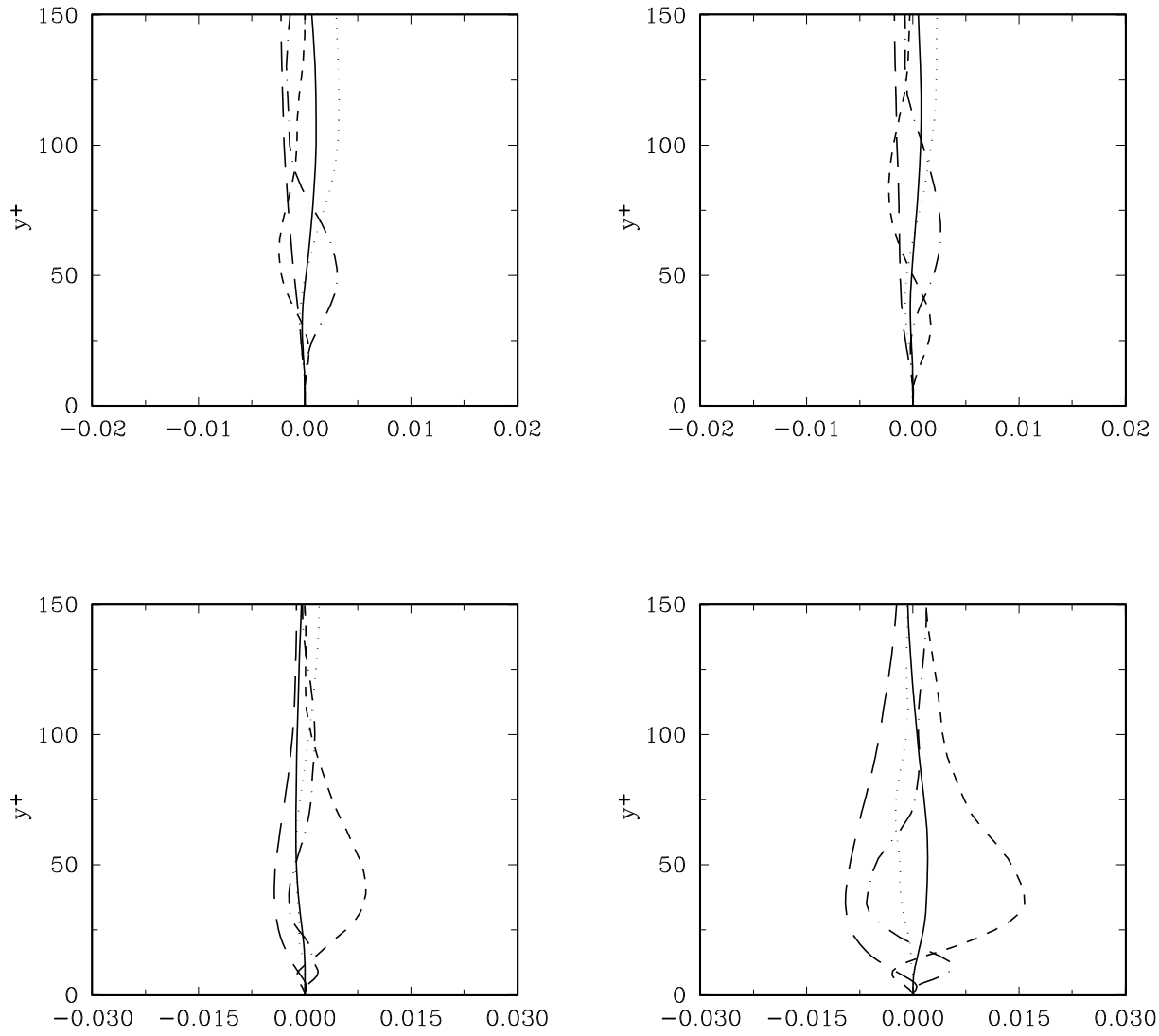

Figure 29. Terms in the balance of $\overline{v'^2}$, with the error term combined with convection. As Figure 23.

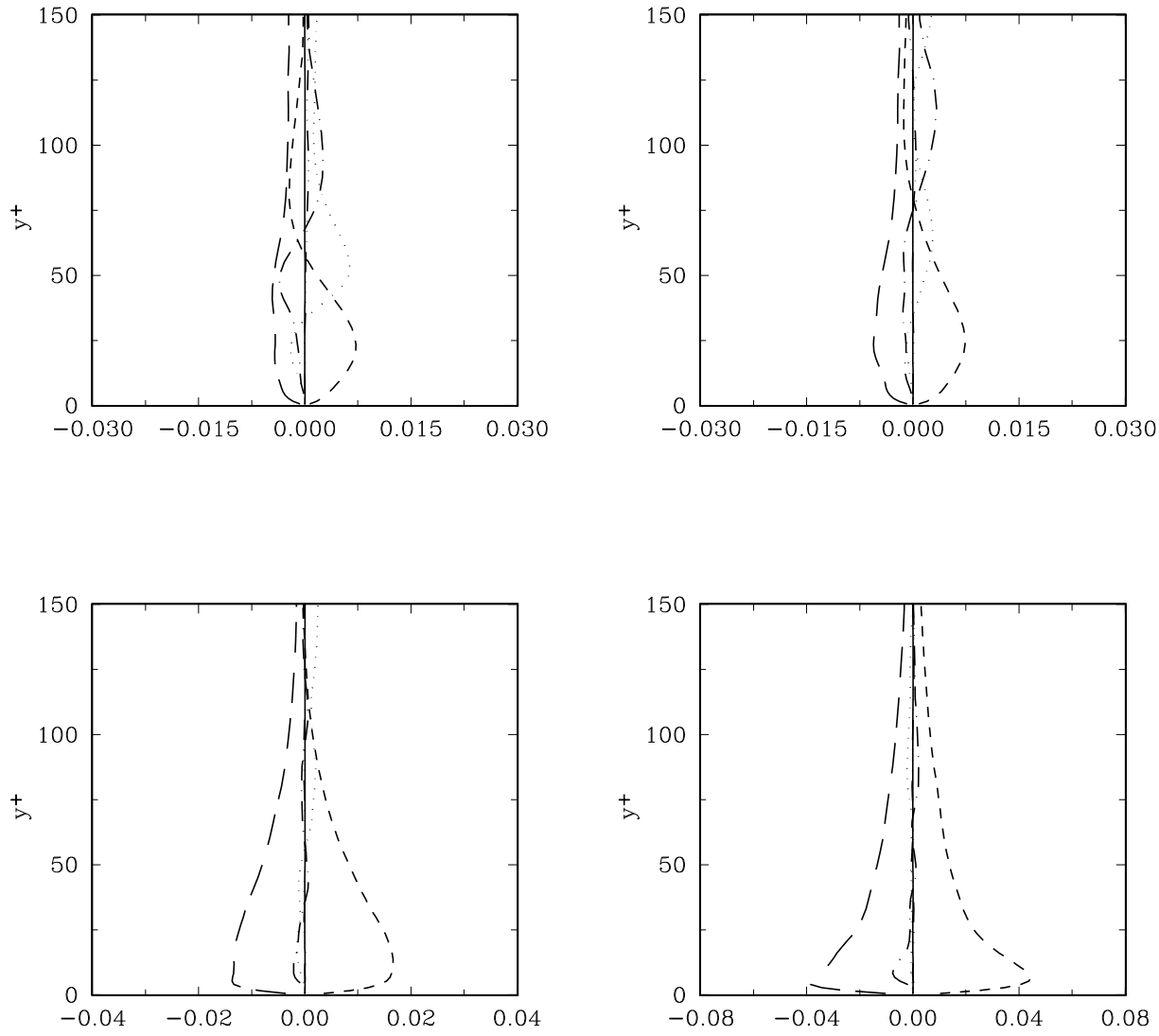

Figure 30. Terms in the balance of $\overline{w'^2}$. As Figure 22.

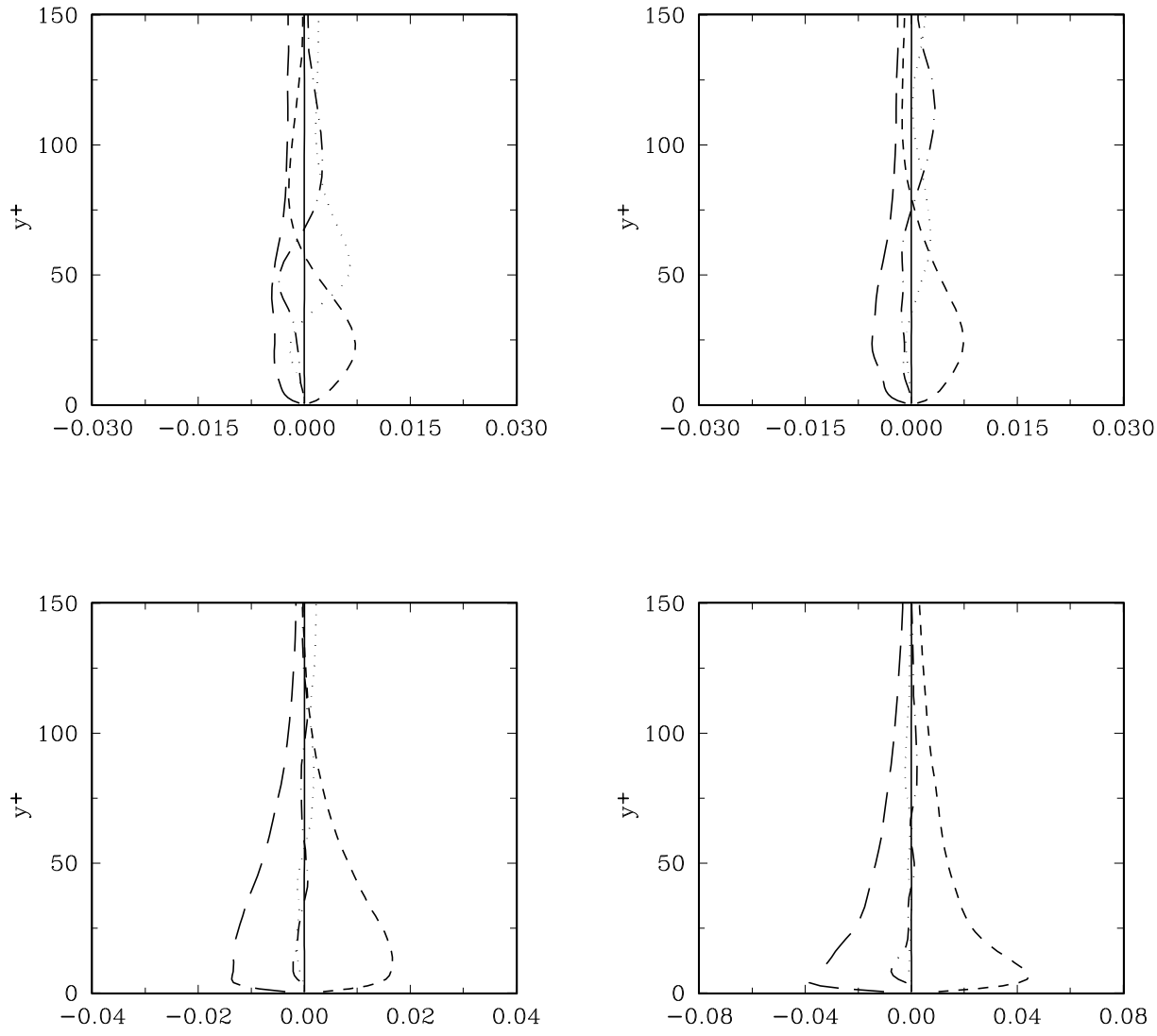

Figure 31. Terms in the balance of $\overline{w'^2}$, with the error term combined with convection. As Figure 23.

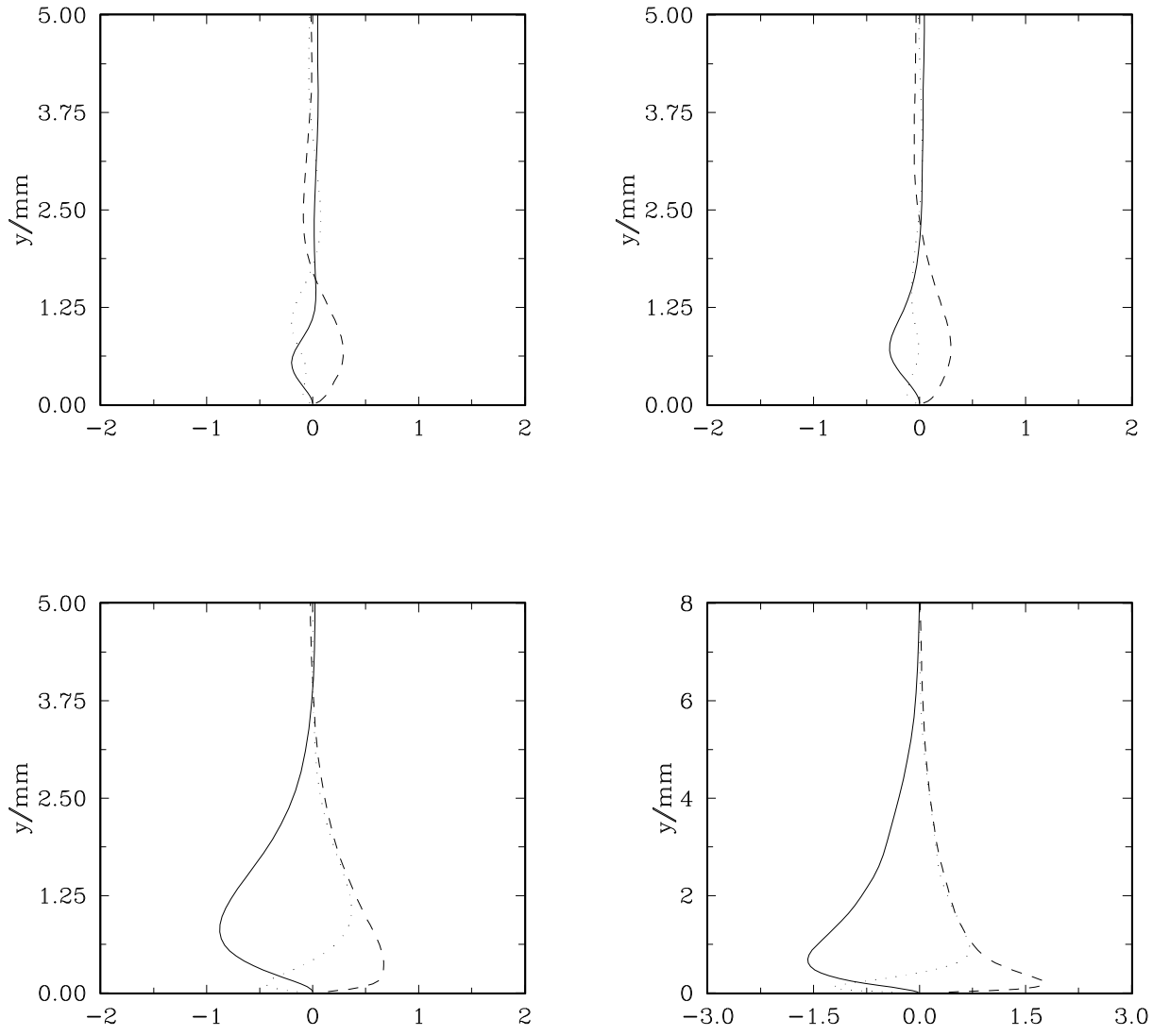

Figure 32. Pressure-strain terms in the balances of diagonal stresses: solid line, $\overline{u'^2}$; dotted line, $\overline{v'^2}$; dashed line, $\overline{w'^2}$.